Available online at www.sciencedirect.com

ScienceDirect

Journal of Nutritional Biochemistry 112 (2023) 109240

Journal of Nutritional Biochemistry

RESEARCH PAPER

Blood orange juice intake modulates plasma and PBMC microRNA expression in overweight and insulin-resistant women: impact on MAPK and NFκB signaling pathways

Vinícius Cooper Capetini[a,b], Bruna J. Quintanilha[a,b], Dalila Cunha de Oliveira[c], Alessandra Harumi Nishioka[d,b], Luciene Assaf de Matos[c], Ludmila Rodrigues Pinto Ferreira[e], Frederico Moraes Ferreira[f], Geni Rodrigues Sampaio[a], Neuza Mariko Aymoto Hassimotto[d,b], Franco Maria Lajolo[d,b], Ricardo Ambrósio Fock[c], Marcelo Macedo Rogero[a,b,*]

[a] Department of Nutrition, School of Public Health, University of São Paulo, São Paulo, Brazil
[b] Food Research Center (FoRC), CEPID-FAPESP (Research Innovation and Dissemination Centers São Paulo Research Foundation), São Paulo, Brazil
[c] Department of Clinical and Toxicological Analysis, School of Pharmaceutical Sciences, University of São Paulo, São Paulo, SP, Brazil
[d] Department of Food Science and Experimental Nutrition, School of Pharmaceutical Sciences, University of São Paulo, São Paulo, Brazil
[e] Morphology Department, Institute of Biological Sciences of the Federal University of Minas Gerais (ICB/UFMG), Belo Horizonte, Brazil
[f] LIM50, Division of Pathology, University of São Paulo School of Medicine, São Paulo, Brazil

Received 29 January 2022; received in revised form 28 July 2022; accepted 12 October 2022

Abstract

Blood orange consumption presents potential health benefits and may modulate epigenetic mechanisms such as microRNAs (miRNAs) expression. MiRNAs are non-coding RNAs responsible for post-transcriptional gene regulation, and these molecules can also be used as biomarkers in body fluids. This study was designed to investigate the effect of chronic blood orange juice (BOJ) intake on the inflammatory response and miRNA expression profile in plasma and blood cells in overweight women. The study cohort was comprised of twenty women aged 18–40 years old, diagnosed as overweight, who consumed 500 mL/d of BOJ for four weeks. Clinical data were collected at baseline and after 4 weeks of juice consumption, *e.g.,* anthropometric and hemodynamic parameters, food intake, blood cell count, and metabolic and inflammatory biomarkers. BOJ samples were analyzed and characterized. Additionally, plasma and blood cells were also collected for miRNA expression profiling and evaluation of the expression of genes and proteins in the MAPK and NFκB signaling pathways. BOJ intake increased the expression of miR-144-3p in plasma and the expression of miR-424-5p, miR-144-3p, and miR-130b-3p in peripheral blood mononuclear cells (PBMC). Conversely, the beverage intake decreased the expression of let-7f-5p and miR-126-3p in PBMC. Computational analyses identified different targets of the dysregulated miRNA on inflammatory pathways. Furthermore, BOJ intake increased vitamin C consumption and the pJNK/JNK ratio and decreased the expression of *IL6* mRNA and NFκB protein. These results demonstrate that BOJ regulates the expression of genes involved in the inflammatory process and decreases NFκB-protein expression in PBMC.

Keywords: microRNA; blood orange; inflammation; overweight; flavonoids.

1. Introduction

Overweight affects more than 1.9 billion adults worldwide [1]. It is estimated that 2.8 million people die each year from conditions that stem from overweight and obesity, including non-communicable diseases (NCD), such as cardiovascular diseases (CVD) and type 2 diabetes (T2D) [2]. A dietary pattern high in ultra-processed foods, saturated fatty acids (SFA), and refined carbohydrates, such as those found in the Western diet, is mainly responsible for triggering excess weight and its related comorbidities [3–5].

Hypercaloric diets are related to gut microbiota dysbiosis and the increase of gut permeability to lipopolysaccharides (LPS), large inflammatory molecules found in the outer membrane of Gram-negative bacteria [6,7]. Through its interaction with Toll-like receptor 4 (TLR4), LPS can activate mitogen-activated protein kinase (MAPK) and nuclear factor kappa B (NFκB) signaling pathways, which increase the expression of the inflammatory cytokines and impairs insulin signaling [8–10]. Conversely, SFA can also induce TLR4-independent activation of MAPK and NFκB pathways components by endoplasmic reticulum stress and accumulation of reactive oxygen species (ROS) [8,11–13]. In addition, adipocyte hy-

* Corresponding author at: Marcelo Macedo Rogero, University of São Paulo, São Paulo, Brazil.
E-mail address: mmrogero@usp.br (M.M. Rogero).

https://doi.org/10.1016/j.jnutbio.2022.109240
0955-2863/

pertrophy is accompanied by the infiltration and differentiation of monocytes into M1 macrophages, leading to the release of cytokines, lipolysis, and the recruitment of other immune cells, including further monocytes and neutrophils [14–16]. These disorders trigger metabolic inflammation [17], which is widely associated with overweight and obesity and etiologically contributes to its related comorbidities [10,18–20].

Healthy diets, higher in fruits and vegetables, are associated with the reduction of cardiovascular risk [21,22]. In humans, orange juice intake prevented the oxidative and pro-inflammatory stress of a high-fat, high-carbohydrate meal in the post-prandial time [23]. These effects were attributed mainly to naringenin and hesperidin, the main flavanones found in oranges [24,25]. Blood orange [*Citrus sinensis* (L.) Osbeck], in particular, is an abundant source of flavanones, anthocyanins, carotenoids, and vitamin C [26,27], which are strongly associated with antioxidant and anti-inflammatory functions [24,28–32]. In addition, blood orange juice (BOJ) intake improved endothelial function by increasing the bioavailability of nitric oxide in overweight and obese men [33], reduced total cholesterol and LDL-cholesterol levels in obese women [34], improved antioxidant activity in healthy smokers [35], and BOJ extract supplementation reduced body mass index (BMI) in overweight volunteers [36]. However, the molecular mechanisms by which these effects are triggered remain poorly understood.

Advances in the genomics field show that nutrients and bioactive compounds found in orange juice can modulate epigenetic mechanisms, such as microRNA (miRNA) expression [37–42,35]. MiRNAs are small non-coding RNAs that participate in post-transcriptional control of gene expression. It is estimated that more than 60% of gene expression in humans is regulated by miRNAs [43], which are involved in the regulation of different signaling pathways [6,44–47]. In addition, miRNAs can be found in serum, plasma, and other body fluids and have been identified as potential biomarkers of disease states, such as NCD [48,49]. Thus, there is an increased interest in developing novel therapies based on the modulation of miRNA expression [50,51] and, consequently different types of foods and nutritional factors could be beneficial for this purpose, especially in diet-induced comorbidities [6,35,37,42,52,53].

Therefore, considering the anti-inflammatory potential of blood orange and the possible effect of its compounds on epigenetic control, we analyzed the effect of BOJ intake on the miRNA expression profile in plasma and peripheral blood mononuclear cells (PBMC) samples in overweight women following a Western dietary pattern. We also measured plasma levels of inflammatory biomarkers and the expression of genes and proteins in the MAPK and NFκB signaling pathways in blood cells. In addition, we used computational analyses to identify potential miRNA targets in the MAPK and NFκB pathways, as well as potential canonical pathways regulated by dysregulated miRNAs in PBMC after BOJ intake.

2. Materials and methods

2.1. Subjects and study design

Twenty women aged 18–40 years old, diagnosed as overweight (BMI 25–29.9 kg/m^2), were recruited for this interventional and chronic study. The participants' exclusion criteria were: men; aged < 18 or > 40 years old; BMI < 25 or > 29.9 kg/m^2; athletes; diagnosis of metabolic diseases or chronic gastrointestinal disorders; use of medicines to control inflammation, plasma lipid profile, or systemic blood pressure; use of supplements or any medicine that could interfere with the intestinal microbiota; frequent consumption of orange juice; smoker; pregnant; and who were participating in another study.

The interventions occurred in Health Center Geraldo Horacio de Paula Souza, School of Public Health, University of São Paulo, Brazil. Samples and data were collected at baseline and 4 weeks after daily ingestion of 500 mL of BOJ. Following 7 d without alcohol consumption, 48 hours without exercise, and 12 hours of fasting, measurements were made of blood pressure (Omron HEM-7113, Kyoto, Japan), glycemia (Accu-Chek Active, Basel, Switzerland), weight, height, and waist and hip circumference (Fig. 1).

A total of 30 mL of blood samples were collected in tubes containing ethylenediaminetetraacetic acid (EDTA), sodium citrate, and gel and clot activator. The analysis of hemoglobin concentration was measured by an automated system (Horiba ABX, Montpellier, France). The hemoglobin concentration of less than 12 g/dL was adopted as a criterion of infeasibility to participate in the study since it may be related to anemia [54].

Twenty-four hour dietary recalls (24hR) were conducted to estimate nutrient intake using the Brazilian Food Composition Table (TACO) [55], the food database of the US Department of Agriculture (USDA) [56], and food labels. The estimated total energy requirement of the participants was calculated using equations proposed by the Institute of Medicine (IOM) [57]. The experimental protocol was approved by the Ethics Research Committee of the School of Public Health at the University of São Paulo (CAAE: 69382217.9.0000.5421) and registered on the Brazilian Clinical Trials Registry (UTN: U1111-1241-4665). All volunteers signed a written informed consent.

2.2. Moro blood orange juice characterization

Pasteurized BOJ (Moro variety) was supplied by Fundecitrus (Araraquara, São Paulo, Brazil). The juice was divided into 1 L flasks and immediately stored at -18°C. The soluble solids (SS °Brix) content was evaluated with a portable digital refractometer (model DR 201-95) (Krüss Optronic, Hamburg, Germany), and the pH was measured by a pH meter model Metrohm 827 pH Lab Meter Swissmade (Metrohm AG, Herisau, Switzerland). Total phenolics were measured on a spectrophotometer (Hewlett Packard, model 8453) at 765 nm by the method described by Swain and Hillis [58]. The organic acids were analyzed by high-performance liquid chromatography (HPLC) on Agilent 2100 equipment with diode array detector (DAD), using a μBondpack C18 column (300 mm × 3.6 mm id) (Waters, Milford, USA), with a mobile phase of 0.1% phosphoric acidand a flow rate of 0.5 mL.min^{-1}, monitored at 210 nm [59].

The soluble sugars were analyzed by HPLC coupled to a pulsed amperometric detector [60]. The content of total dietary fiber and fractions were measured according to the method prescribed by the Association of Official Analytical Chemists (AOAC) (AOAC 991.43) [61]. The antioxidant capacity was evaluated by oxygen radical assay capacity (ORAC), as described by Prior et al [62], and by diphenylpicrylhydrazyl (DPPH), as described by Brand-Williams, Cuvelier, and Berset [63]. The plates were read on Synergy H1 (Biotek Instruments, Winooski, USA) at 485 nm/525 nm in the ORAC assay and 517 nm in the DPPH assay.

The identification of anthocyanins and other flavonoids was performed by liquid chromatography-electrospray ionization tandem mass spectrometry (LC-ESI-MS/MS) and quantification of these compounds was performed by HPLC on Agilent 2100 equipment with DAD using a Prodigy 5 μm ODS3 column (250 × 4.60 mm) (Phenomenex Ltd. - Cheshire, UK), with a flow rate of 1 mL.min^{-1} and 0.8 mL.min−1 at 25°C for flavonoids and anthocyanins, respectively, as described by Nishioka et al. [64]. The compounds were identified by comparing the mass spectra obtained with commercial standards and/or literature data. Quantification was performed using a calibration curve with identified flavanones (at 280 nm) and anthocyanins (at 525 nm) standards.

Carotenoids were separated by HPLC-DAD-MS/MS on a C30 YMC column (5 μm, 250 mm × 4.6 mm), using a gradient elution of methanol and tert-methyl butyl ether as described by Petry and Mercadante [65]. Carotenoids were identified according to UV-vis and MS/MS spectra characteristics and comparison with standards. Quantification was done by calibration curves of (all-*E*)-lutein, (all-*E*)-zeaxanthin, (all-*E*)-β-cryptoxanthin, and (all-*E*)-β-carotene; *Z* isomers were quantified using the curve of the corresponding (all-*E*)-isomer; (all-*E*)-violaxanthin, (all-*E*)-antheraxanthin, (all-*E*)-luteoxanthin, mutatoxanthin, and their (*Z*)-isomers were quantified using the curve of lutein; the (all-*E*)-β-carotene curve was used for phytoene, phytofluene, and ζ-carotene quantification.

2.3. Blood sampling and analysis

Whole blood tubes were centrifuged at 1200 x g for 15 min at room temperature. Plasma and serum were aliquoted and kept frozen at -80°C until analysis. Plasma from EDTA tubes was used for the analysis of microRNA, lipopolysaccharides (LPS), lipopolysaccharide-binding protein (LBP), soluble CD14 (sCD14), inflammatory biomarkers, insulin, leptin, and adiponectin. Plasma from the sodium citrate tubes was used for the analysis of fibrinogen. The serum from tubes with gel and clot activator was used for the analysis of the lipid profile, aspartate transaminase (AST), alanine transaminase (ALT), gamma-glutamyltransferase (GGT), C-reactive protein (CRP), amylase, urea, creatinine, and minerals. Insulin levels were determined with enzyme-linked immunoassay (ELISA) kits (Insulin Accubind Elisa Kit; Monobind Inc., Lake Forest, USA) according to the manufacturer's instructions. The tissue sensitivity to insulin was assessed by homeostasis model assessment (HOMA). The fasting glycemia and insulin levels were used to calculate the insulin sensitivity index (HOMA-IR), using the following equation: HOMA-IR = glucose × insulin ÷ 22.5 [66].

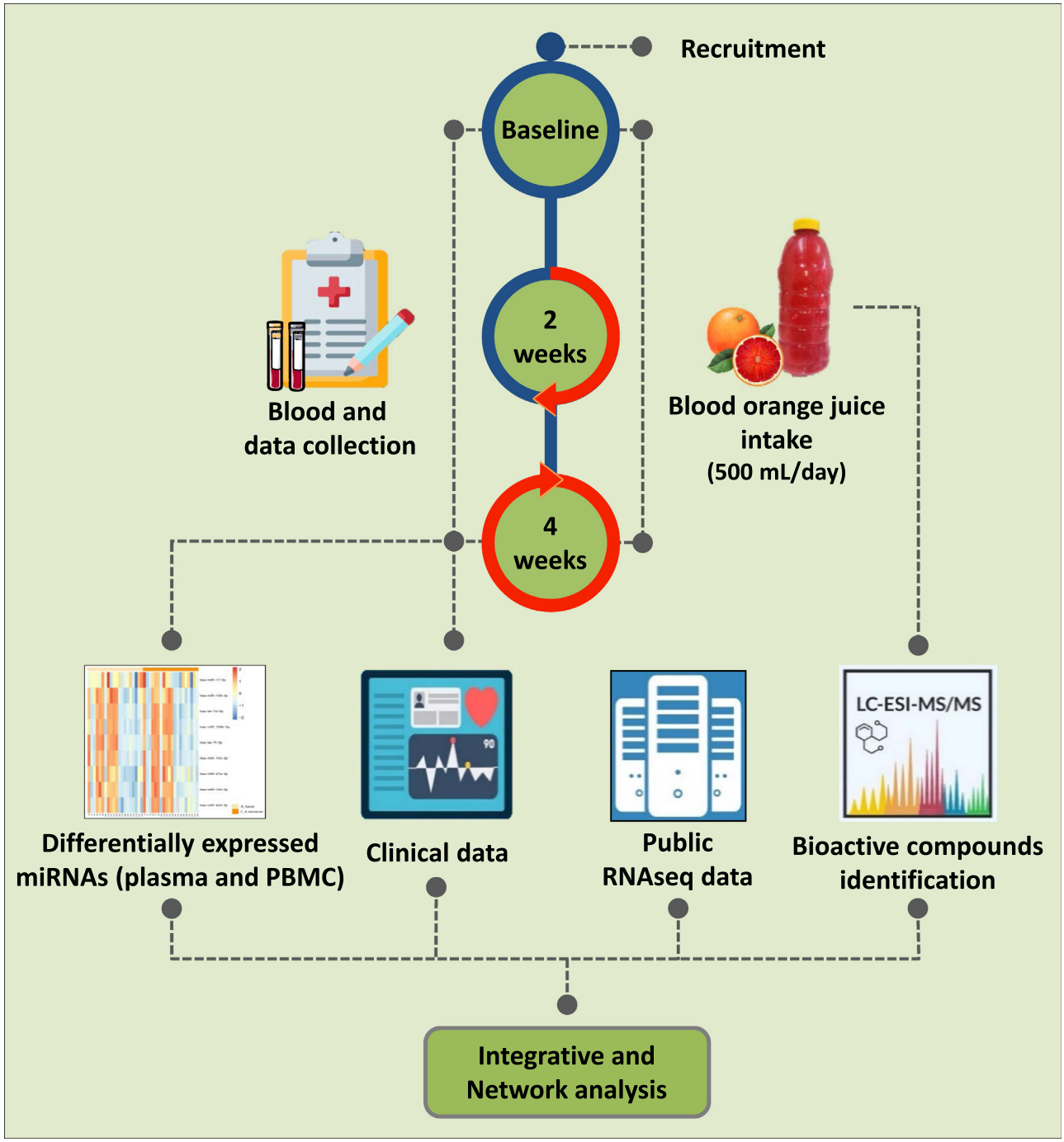

Fig. 1. Flow diagram of the study protocol. Twenty overweight women were recruited for a 4-week consumption period of daily 500 mL Moro blood orange juice. Peripheral blood and clinical data were obtained before the beginning of the intervention phase (baseline) and after 4 weeks. MiRNA profiling was performed with plasma and PBMC from baseline and 4 weeks. The other clinical parameters were also collected with blood from baseline and 4 weeks. Bioactive compounds from the blood orange juice were identified by LC-ESI-MS/MS. Integrative, pathway, and network analysis were performed integrating miRNA-Public RNAseq data, clinical parameters, and orange juice compound. LC-ESI-MS/MS, liquid chromatography-electrospray ionization tandem mass spectrometry; PBMC, peripheral blood mononuclear cells.

LPS levels were analyzed using a commercially available kit [Cambrex Limulus Amebocyte Lysate (LAL) kit; Lonza Inc, Walkersville, MD, USA]. LBP and sCD14 levels were analyzed by ELISA kits HK320-02 and HK315-02 (Hycult Biotech, Uden, Netherlands), respectively. Interleukin (IL)-6, IL-10, tumor necrosis factor α (TNF-α), monocyte chemoattractant protein 1 (MCP1), soluble vascular cell adhesion molecule 1 (sVCAM-1), soluble intercellular adhesion molecule 1 (sICAM-1), leptin and adiponectin were analyzed by DuoSet ELISA kits (R&D Systems, Minneapolis, USA). All analyses were performed according to the manufacturer's instructions.

Serum levels of total cholesterol, low-density lipoprotein (LDL), high-density lipoprotein (HDL), triacylglycerol, CRP, fibrinogen, D-dimer, ALT, AST, GGT, amylase, urea, creatinine, and minerals were measured by an automated dosing system (Roche, Cobas 6000 analyzer, Basel, Switzerland) in the Clinical Analysis Laboratory of the University Hospital of São Paulo. Non-HDL-cholesterol was calculated using

total cholesterol (TC) less HDL [67]. The AST/ALT ratio was calculated and included as an index for the assessment of liver health [68].

2.4. Blood cell count

Blood samples were collected with EDTA as described above, and a blood cell count was performed using an automated system (Horiba ABX, Montpellier, France). The morphological and leukocyte differential analyses were performed on blood smears stained by the May-Grünwald-Giemsa (Merck, Darmstadt, Germany) technique.

2.5. Flow cytometry

Whole blood was collected on EDTA tubes and centrifuged for plasma separation, as described above, to access the immunophenotype of blood cells. Red blood cells were removed by adding 2 mL of Red Cell Lysis Buffer (BD Pharmingen, Becton Dickinson, New Jersey, USA) following the manufacturer's instructions, and cells were washed twice using phosphate-buffered saline (PBS). Flow cytometry was used to determine the percentage fraction of blood cells that were positively labeled with anti-CD4 (PE) (#555347), anti-CD8 (APC) (#553035), anti-CD14 (APC) (#555399), anti-CD11b (PE-Cy7) (#552850) and anti-CD18 (FITC) (#555923) antibodies. Negative controls were performed by the fluorescence minus one (FMO) strategy. All antibodies were purchased from eBioscience (San Diego, CA, USA) or BD Biosciences. Samples were incubated at 4°C in the dark for 30 min. Cells were washed with PBS and resuspended in 0.5 mL of PBS in the dark until flow cytometric analysis. Once labeled, 1×10^4 cells were acquired by flow cytometry. The flow cytometry strategy used is shown in the supplementary information (Supplementary Figure S1). Data were acquired on a FACS Canto II (FACScan, Becton Dickinson, New Jersey, USA), and FlowJo 10 software (Tree Star Inc., Ashland, USA) was used for data analysis.

2.6. PBMC and PMN isolation

After plasma removal, the blood remaining in the EDTA tubes was reconstituted with the same volume of sterile phosphate-buffered saline (PBS), carefully homogenized, and transferred to the 50 mL ACCUSPIN System-Histopaque-1077 tubes (Sigma-Aldrich, St. Louis, USA). PBMC were separated using tube centrifugation at 1000 x g for 10 min at 4°C. The cells were distributed as follows: 4×10^6 cells for miRNA extraction; 1×10^6 cells for mRNA extraction and the remaining cells for protein extraction. The samples were frozen at -80°C until analysis.

For polymorphonuclear neutrophils (PMN) isolation, another EDTA tube containing whole blood was used. PMN were isolated using a modified Percoll method [69]. A Percoll gradient was made by slowly adding 3 mL of 70% Percoll solution (Sigma-Aldrich, St. Louis, USA) over 3 mL of 60% Percoll solution, both diluted in Hank's balanced salt solution-EDTA [without calcium, with magnesium, phenol red, and sodium bicarbonate, pH 7.2, 15 mM EDTA, 1% bovine serum albumin (BSA)] (HBSS, GIBCO, Grand Island, NY, USA). Subsequently, 3 mL of whole blood was added slowly over the Percoll gradient and was centrifuged at 400 x g for 20 min at 22°C, with an acceleration/ brake of 2 m/s^2. After centrifugation, a halo between the 70% and 60% Percoll solutions containing PMN was harvested into 1% BSA-coated tubes after the cells from the upper phases were carefully removed. After one wash with 2 mL HBSS-EDTA + 1% BSA, residual red blood cells were removed by adding 2 mL Red Cell Lysis Buffer (BD Pharmingen, Becton Dickinson, New Jersey, USA) to the tube. PMN were then washed with HBSS by centrifugation at 400 x g for 10 min at 22°C. After washing, the PMN were resuspended in 1 mL of HBSS.

2.7. RNA isolation and quantitative real-time PCR

Total RNA was obtained from 1×10^6 PBMC using the Mini Kit RNeasy extraction kit with DNase treatment (Qiagen, Germantown, USA), according to the manufacturer's protocol. RNA quality was evaluated by the A260nm/A280nm ratio [70]. The absorbance was measured with a NanoVue Plus spectrophotometer (Biochrom, Holliston, USA), and samples whose absorbance ratios were in the range between 1.9 and 2.1 were considered appropriate for use. Total RNA was reverse-transcribed into cDNA using the High Capacity cDNA Reverse Transcription Kit with RNase Inhibitor (Applied Biosystems, Foster City, USA) in the Research PTC-100 Thermal Cycler (MJ Research, St. Bruno, Canada) according to the manufacturer's protocol. cDNA samples were stored at -40°C until real-time PCR was performed.

One microliter of each cDNA (10 ng/μL) sample was amplified in the TaqMan Fast Universal master mix (Applied Biosystems, Foster City, USA) with optimized concentrations of the primer sets for *RELA* (Hs01042014_m1), *NFKB1* (Hs00765730_m1), *NFKBIA* (Hs00153283_m1); *TNF* (Hs00174128_m1), *IL1* (Hs01555410_m1), *IL6* (Hs00174131_m1), *IL10* (Hs00961622_m1), *TLR2* (Hs00152932_m1) e *TLR4* (Hs00152939_m1). Gene expression was normalized by *RNA18S5* (Hs03928990_g1). The primer set was purchased from Applied Biosystems. The amplification reaction was performed using StepOnePlus (Applied Biosystems, Foster City, USA). All reactions were performed in duplicate, and negative controls were used for each reaction plate. The gene expression was quantified according to the ΔΔCt method [71].

2.8. MiRNA extraction, real-time qPCR, and miRNA profiling

Total RNA was extracted and purified from 200 μL of plasma using the miRCURY RNA isolation kit for biological fluids (QIAGEN, Hilden, Germany) and from 4×10^6 cells using the QIAGEN miRNeasy Mini Kit (QIAGEN, Hilden, Germany) according to the manufacturer's instructions. Artificial RNA (UniSp2, UniSp4, UniSp5) was added to buffer lyses for calibration of RNA extraction [72]. Two microliters of RNA from plasma and 10 ng of RNA from PBMC were reverse transcribed in 10 μL reactions using the miRCURY LNA Universal RT microRNA PCR, Polyadenylation, and cDNA synthesis kit (QIAGEN, Hilden, Germany). Plasma and cellular cDNA were diluted 50x and 100x, respectively, and assayed in 10 μL PCR reactions according to the manufacturer's instructions. Reverse transcription was performed including a sample of artificial RNA (UniSp6) to control the cDNA synthesis [72]; each microRNA was assayed once by qPCR on the microRNA Ready-to-Use PCR, Pick and Mix using ExiLENT SYBR Green master mix (QIAGEN, Hilden, Germany). A sample of artificial RNA (UniSp3) was used to monitor PCR efficiency [72].

MiRNA profiling experiments were done in two steps. In a first analysis, two panels that identify the miRNAs most commonly expressed in plasma (miRCURY LNATM Universal RT microRNA PCR Serum/Plasma Focus panel) and leukocytes (miRCURY LNA Universal RT microRNA PCR custom Pick and Mix panel) (QIAGEN, Hilden, Germany) were used to assess the profiles of 179 and 137 miRNA in plasma (n=8) and PBMC (n=8) samples, respectively (Supplementary Table S1 and S2), according to the manufacturer's protocols. In a second analysis, the differentially expressed miRNAs (P-value <.05) identified previously and further miRNAs in plasma (miR-30e-5p, miR-15a-5p, miR-101-3p, and miR-150-5p) and PBMC (mir-142-3p and miR-17-5p), previously described as involved in the inflammatory process [73–78], were quantified in new samples of plasma (n=12) and PBMC (n=12) from the same cohort. Negative controls, excluding the template from the reverse transcription reaction, were performed and profiled like the samples. The amplification was performed in a LightCycler 480 Real-Time PCR System (Roche, Basel, Switzerland) in 384-well plates. The amplification curves were analyzed using the Roche LC software, both for the determination of Cq (calculated by the second derivative method) and for melting curve analysis. Hemolysis in plasma samples was checked by the ΔCq hsa-miR-23a-to-hsa-miR-451 ratio, which increases the risk of being positive if > 7 [72].

Real-time PCR amplification (Cq values) was normalized by the global mean in the first analysis and by hsa-miR-222-3p and hsa-miR-21-5p in the second analysis for plasma and PBMC samples, respectively. Differentially expressed miRNAs (P-value <.05 and absolute fold change ≥1.25) were identified by comparing the control and four-week groups using the R/Bioconductor package LIMMA [79].

2.9. Pathway and network analysis

Differentially expressed miRNAs were uploaded to Ingenuity Pathway Analysis (IPA) software (QIAGEN, Aarhus, Denmark) for in silico analysis. The miRNA target filter tool was used to identify potential targets of the dysregulated miRNAs, based on experimentally validated interactions extracted from TarBase and miRecords databases, and predicted miRNA-mRNA interactions from TargetScan database. Highly predicted targets of miRNAs were identified by the presence of conserved sites that match the seed region of each miRNA. On the other hand, moderately predicted targets are identified by sites with mismatches in the seed region that are compensated by conserved 3′ pairing [43] and centered sites [80]. MAPK and NFκB signaling pathways were built with the differentially expressed miRNAs and their validated and/or predicted targets, showing the molecular interactions between these miRNAs and their target mRNAs.

2.10. Protein extraction and western blotting

PBMCs and PMN were collected as described above and lysed in RIPA buffer (Sigma-Aldrich, St. Louis, USA) supplemented with phosphatase (NaF 1 M and sodium orthovanadate 10 mM) and protease inhibitors (PMSF 22,96 mM and Protease Inhibitor Cocktail, Sigma-Aldrich, St. Louis, USA). Protein expression was measured using the Pierce BCA protein analysis kit (Thermo Fisher Scientific, Waltham, USA), according to the manufacturer's instructions. The protein extracts were boiled for 10 min in a water bath and maintained at -80°C for future electrophoresis analyses.

For PBMC and PMN analyses, 10 μg and 30 μg of total proteins, respectively, were resolved by electrophoresis on 10% TGX FastCast polyacrylamide gel (BioRad, Hercules, USA) in a Mini-PROTEAN mini gel device (BioRad, Hercules, USA). After electrophoresis, the proteins were electrically transferred to nitrocellulose membranes for 10 min in the Power Blotter System (Life Technologies, Shanghai, China). The membranes were incubated at room temperature for 1 h, under agitation, in TSBT (Tris 10 mM, NaCl 1.5 mM, pH 7.6, Tween 0,1%) with 5% BSA to block the nonspecific binding of antibodies to the membranes. For PBMC analyses, membranes were incubated overnight at 4°C with primary antibodies against total TAK1 (#5206), pTAK1 (Thr184/187) (#4508), IKKβ (#8943), pIKK (Ser176/180) (#2697), JNK (#3708), pSAPK/JNK (Thr183/Tyr185) (#4668), IκBα (#9242), pIκBα (Ser32) (#2859), NFκB p65 (#4764), pNFκB (Ser536) (#3031), and β-actin (#8457) (Cell

Table 1
Volunteers' profile

	Mean±SD
Age (years)	27.5±6.5
Weight (kg)	74.4±6.4
Height (m)	1.64±0.07
Body mass index (kg/m^2)	27.8±1.5
Estimated energy requirement (Kcal/d)	2124±137
Waist circumference (cm)	89.1±5.0
Waist-hip ratio	0.83±0.05
Systolic blood pressure (mm Hg)	113±9
Diastolic blood pressure (mm Hg)	69.7±8.2
HOMA-IR	3.05±1.52
Hemoglobin (g/dL)	13.6±1.3

All values are mean±standard deviation (SD), n=20.
Abbreviation: HOMA-IR, homeostasis model assessment of insulin resistance.

Signaling Technology, Beverly, MA, USA). For PMN analyses, membranes were incubated with antibodies against Stat3 (sc-8019), pStat3 (sc-8059) NFκB p65 (sc-372), pNFκB (sc-33039) (Santa Cruz Technology, CA, USA), and β-actin (#8457) (Cell Signaling Technology, Beverly, MA, USA). The antibodies were diluted (1:1000) in TSBT with 3% BSA. Following that, membranes were incubated with a secondary HRP-conjugated antibody (Cell Signaling Technology, Beverly, USA) for 60 min at room temperature and then incubated with a solution containing the chemiluminescence reagent Clarity Western ECL Substrate (BioRad, Hercules, USA). The intensity of the colored bands was determined by densitometry using ImageQuant LAS 4000 (GE Healthcare, Chicago, USA). Band intensities were normalized to β-actin to determine the relative protein expression.

2.11. Statistical analyses

Data are presented as the mean ± SD (standard deviation) and were analyzed with GraphPad Prism7 software (GraphPad Software, Inc., La Jolla, CA, USA). The fourth week was evaluated by paired data analysis concerning the baseline time. The variables with normal distribution, shown by the D'Agostino & Pearson normality test, were evaluated by the paired t-test. For variables that did not have a normal distribution, the difference between the time averages was assessed by the Wilcoxon matched-pairs test. A P-value <.05 was adopted to reject the null hypothesis.

3. Results

From an initial cohort of 40 women interviewed, 25 were recruited, as they complied with the first selection criteria. Two volunteers who showed hemoglobin levels lower than 12 g/dL and another who reported the use of the anti-inflammatory drug (ibuprofen) were removed from the current study. Additionally, two volunteers did not complete the three blood draws. Thus, 20 (n=20) women completed the experimental protocol. All volunteers showed overweight, an increased risk of metabolic complications (WC > 80 cm) [81], and an indication of the presence of insulin resistance (HOMA-IR > 2.70) [82] (Table 1).

The characterization of the BOJ is displayed in Table 2. The ingestion of 500 mL of BOJ presents 249.6 kcal, 52.6 g of sugars, 237 mg of vitamin C, 291 mg of flavonoids, and 2541.5 μg of carotenoids. The beverage had an acidic pH, a 6.50% soluble solids content, a total phenolic concentration of 45.7 mg/100 mL, and an antioxidant capacity of 856.73 μmol eq. Trolox/100 mL for ORAC and a percentage of inhibition of 50.70 for DPPH (Table 2). The identification of flavonoids is displayed in supplementary data (Supplementary Figures S2 and S3). The volunteers did not report any intolerance, allergic reaction, or gastrointestinal discomfort due to the beverage intake.

Corroborating the Western dietary pattern [4], the volunteers had cholesterol and SFA intakes higher than recommended, with more than 300 mg/d and more than 10% of total energy intake, respectively [83]. In addition, the fiber intake was lower than the 25 g/d recommended for adult women [57]. On the other hand, BOJ supplementation increased vitamin C intake (P <.001) without changing the intake of calories, macronutrients, cholesterol, or dietary fiber (Table 3).

BOJ intake did not result in significant changes in anthropometric, hemodynamic (Table 4), metabolic profile, or hematological (Supplementary Tables S3 and S4) parameters. However, the beverage intervention increased serum levels of LDL-cholesterol, non-HDL cholesterol, AST, and the AST/ALT ratio (Table 5). Nevertheless, these metabolites were kept within healthy levels: LDL-cholesterol, less than 130 mg/dL; non-HDL cholesterol, less than 100 mg/dL [84]; AST, less than 35 IU/L; and AST/ALT ratio, greater than 1 and less than 2 [68].

Table 2
Characterization of pasteurized Moro blood orange juice

	Mean±SD or Total
Soluble sugars*	
Sucrose	4.84±0.04
Fructose	2.96±0.05
Glucose	2.73±0.08
Total	10.52
pH	4.14±0.00
TSS (°Brix)	6.50±0.00
Total Phenolics†	45.7±0.0
ORAC§	857±3
DPPH‖	50.7 1.1
Vitamin C‡	47.4±0.0
Total Dietary Fiber*	0.31
Flavonoids‡	
Narirutine	4.19±1.24
Hesperidin	36.5±14.2
Didimin	1.90±0.85
Naringin	0.33±0.01
Naringenin	0.11±0.01
Hesperitin	0.09±0.02
Cyanidin-3-O-glycoside	12.2±1.8
Cyanidin-3-O-(6′-malonyl glycoside)	2.89±1.14
Total Flavanones	43.1
Total anthocyanins	15.1
Total Flavonoids	58.2
Carotenoids¶,#	
Violaxanthin ((all-E) + (9Z))	66.1
Luteoxanthin ((all-E) + (9Z) or (9′Z))	77.2
(all-E)-lutein	66.5
Mutatoxanthine (epimer 1, epimer 2 and epimer 3)	72.3
(all-E)- zeaxanthin	31.6
(all-E)-β-cryptoxanthin	59.0
(9Z)- antheraxanthin	40.8
Total carotene ((all-E) + ζ-carotene isomer 1 and 2)	94.8
Total carotenoids	508.3

The values are mean±standard deviation (SD) or total.
Abbreviations: DPPH, 2,2-diphenyl-1-picrylhydrazyl; ORAC, oxygen radical absorbance capacity; TSS, total soluble solids.
* values expressed in g/100 mL.
† values expressed in mg of gallic acid/100 mL
‡ values expressed in mg/100 mL.
§ values expressed in μmol of Trolox equivalents/100 mL.
‖ inhibition percent.
¶ total values expressed in μg/100 mL.
# the values are a sum of the identified isomers.

Table 3
Estimate of the volunteers' daily intake of calories, macronutrients, dietary fiber, and vitamin C at baseline and 4 weeks after daily intake of 500 mL of Moro blood orange juice

	Baseline	4 wk	*P*-value
Total energy intake (kcal)	2227±546	2309±400	.96
Protein (g)	86.2±22.0	88.3±28.9	.80
Protein per kg of body weight (g)	1.17±0.34	1.18±0.37	.92
Total fat (g)	82.9±30.1	84.6±33.3	.96
% SFA in relation to total energy intake	11.8±4.3	11.8±4.3	.62
Cholesterol (mg)	358±202	357±259	.76
Carbohydrate (g)	305±79	289±54	.44
Dietary fiber (g)	20.7±8.9	15.4±6.8	.05
Vitamin C (mg)	55.5±78.9	268±52	<.001

All values are mean±standard deviation (SD), n=20.
Analyzed by paired t-test or Wilcoxon matched-pairs test.
Abbreviations: SFA, saturated fatty acid.

Table 4
Body composition and blood pressure obtained at baseline and 4 weeks after daily intake of 500 mL of Moro blood orange juice

	Baseline	4 wk	*P*-value
Weight (kg)	74.4±6.4	74.7±6.4	.33
Body mass index (kg/m^2)	27.8±1.5	27.9±1.8	.28
Waist circumference (cm)	89.1±5.0	88.5±4.6	.49
Waist-to-hip ratio	0.83±0.05	0.82±0.06	.19
Systolic blood pressure (mm Hg)	113±9	111±10	.24
Diastolic blood pressure (mmHg)	69.7±8.2	67.9±6.1	.26

All values are mean±standard deviation (SD), n=20.
Analyzed by paired t-test or Wilcoxon matched-pairs test.

Regarding gene expression, BOJ decreased *IL6* mRNA expression in PBMC (Fig. 2) and modulated the expression of different miRNAs involved in MAPK and NFκB signaling pathways in plasma and PBMC (Figs. 3 and 4). In the first analysis of miRNA, 3 of the 179 plasma miRNAs analyzed and 7 of the 137 PBMC miRNAs analyzed were differentially expressed after 4 weeks of BOJ intake in comparison to the baseline time (Fig. 3A). All miRNAs that did not present significant differences are shown in the supplementary data (Tables S5 and S6). In the second analysis of miRNA, previously differentially expressed miRNAs, including further miRNAs in plasma and PBMC that are also related to inflammation [73–78], were analyzed in the other study samples from the same cohort. Thus, considering both miRNA analyses, 1 plasma miRNA and 5 PBMC miRNAs showed a significant difference in expression after BOJ intake for 4 weeks in comparison to the baseline time (Fig. 3B, C, D).

The amplification curves for the RNA spike-ins were similar among most samples enabling a reliable comparison between different samples and demonstrating that the processes of RNA extraction, cDNA production, and amplification were done in a homogeneous way (Supplementary Figures S4 and S5). However, sample 18C showed low amplification efficiency, with only two miRNAs detected, which was confirmed by the high Cq level of UniSp6 (Supplementary Figure S4b). In addition, the ΔCq miR-23a-to-miR-451 ratio for the 12C plasma sample was 8.1, which indicates an increased risk of it being affected by hemolysis (Supplementary Figure S6) [72]. Consequently, these samples were removed from the analysis to enable normalization, decreasing the number of plasma samples for miRNA analysis (n=18).

IPA software was used for targeting prediction and pathway analyses. We identified 383 experimentally validated targets of the 5 differentially expressed miRNAs in PBMC. The top 40 canonical pathways most enriched are shown in Fig. 3E. We observed enrichment in canonical pathways related to inflammation, antioxidation, growth factor signaling, and metabolism. Figure 4 shows a representation, in a cellular layout, of the predicted targets of the differentially expressed miRNAs within the MAPK and NFκB signaling pathways.

Considering the great number of targets of the differentially expressed miRNAs related to inflammatory signaling pathways, we tested whether BOJ intake would affect the protein expression of these pathways. We observed that BOJ induced a decrease in the protein expression of NFκB (P <.05) and an increase in the

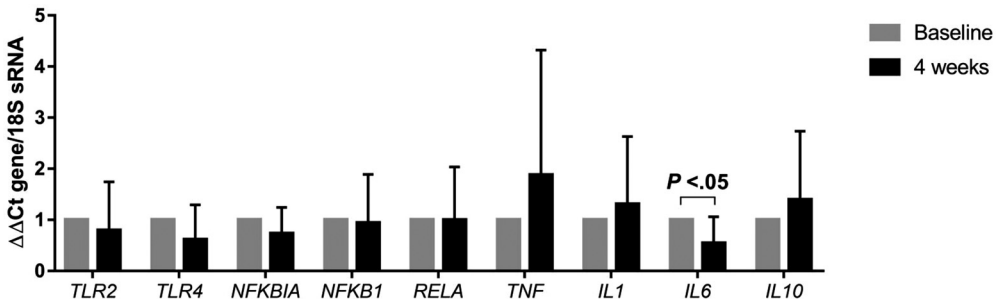

Fig. 2. Effect of daily intake of 500 mL of Moro blood orange juice for 4 weeks on mRNA expression of the inflammatory pathway in PBMC from overweight women. Expression of *TLR2, TLR4, NFKBIA, NFKB1, RELA, TNF, IL1, IL6*, and *IL10*. Values are mean±standard deviation (SD), n=12. Analyzed by paired t-test or Wilcoxon matched-pairs test. *IL*, interleukin; *NFKBIA*, Nuclear factor-kappa B alpha inhibitor; *NFKB1*, nuclear factor kappa B p50 subunit; *RELA*, nuclear factor kappa-B subunit p65; *TLR*, toll-type receptor; *TNF*, tumor necrosis factor-alpha.

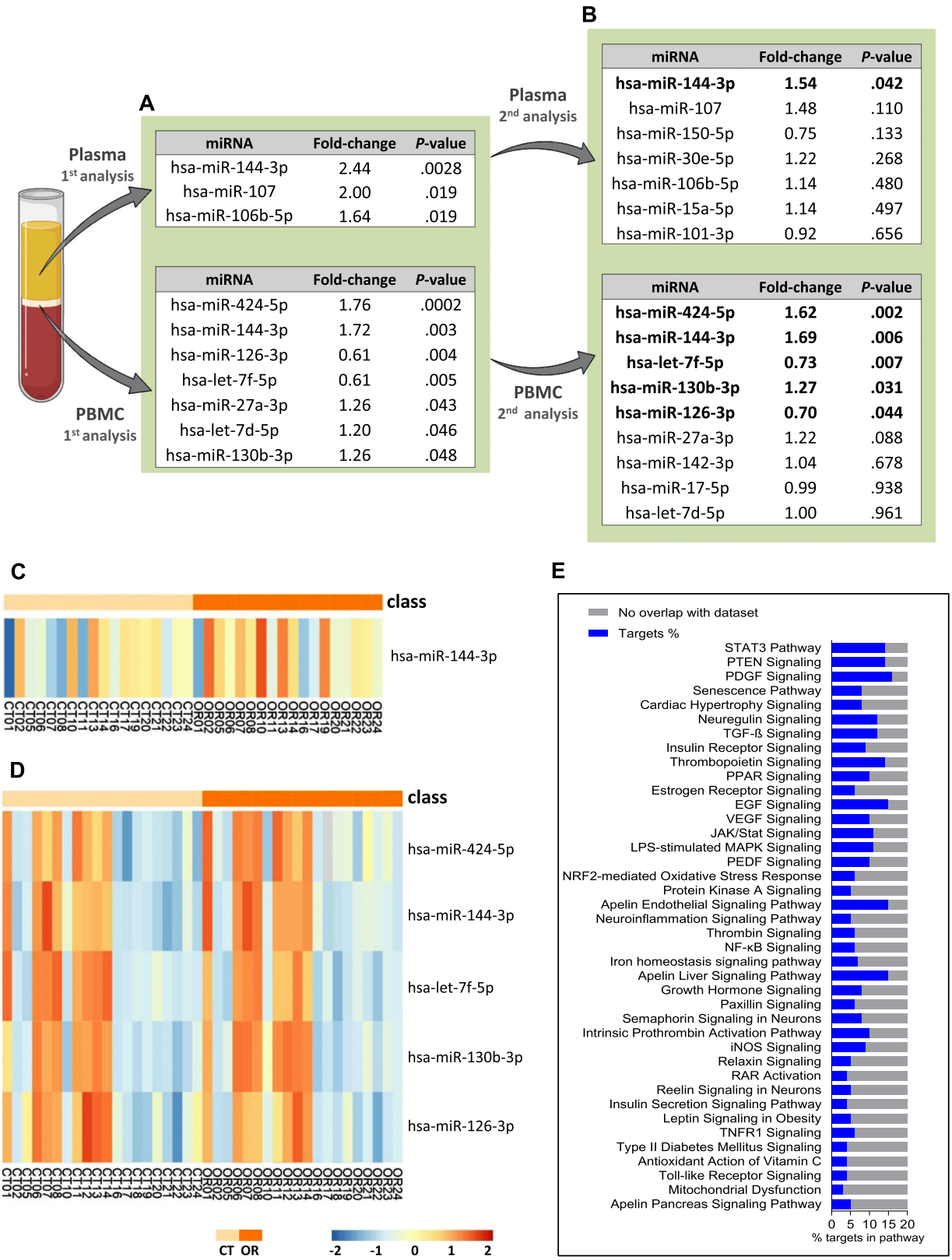

miRNA	Fold-change	*P*-value
hsa-miR-144-3p	2.44	.0028
hsa-miR-107	2.00	.019
hsa-miR-106b-5p	1.64	.019

miRNA	Fold-change	*P*-value
hsa-miR-424-5p	1.76	.0002
hsa-miR-144-3p	1.72	.003
hsa-miR-126-3p	0.61	.004
hsa-let-7f-5p	0.61	.005
hsa-miR-27a-3p	1.26	.043
hsa-let-7d-5p	1.20	.046
hsa-miR-130b-3p	1.26	.048

miRNA	Fold-change	*P*-value
hsa-miR-144-3p	**1.54**	**.042**
hsa-miR-107	1.48	.110
hsa-miR-150-5p	0.75	.133
hsa-miR-30e-5p	1.22	.268
hsa-miR-106b-5p	1.14	.480
hsa-miR-15a-5p	1.14	.497
hsa-miR-101-3p	0.92	.656

miRNA	Fold-change	*P*-value
hsa-miR-424-5p	**1.62**	**.002**
hsa-miR-144-3p	**1.69**	**.006**
hsa-let-7f-5p	**0.73**	**.007**
hsa-miR-130b-3p	**1.27**	**.031**
hsa-miR-126-3p	**0.70**	**.044**
hsa-miR-27a-3p	1.22	.088
hsa-miR-142-3p	1.04	.678
hsa-miR-17-5p	0.99	.938
hsa-let-7d-5p	1.00	.961

Fig. 3. Differentially expressed miRNA profiles in plasma and PBMC, 4 weeks after daily intake of 500 mL of Moro blood orange juice. (A) Differentially expressed miRNA profiles in plasma (n=7) and PBMC (n=8) from the first miRNA analysis. (B) miRNA expression profile in plasma (n=18) and PBMC (n=20) from second miRNA analysis. The supervised heat map illustrates the fold change profile of differentially expressed miRNAs in plasma (C) and PBMC (D), in which columns represent samples and rows represent miRNAs. The color-coded scale illustrates the miRNA relative expression (DCt) after global normalization. Blue indicates expression levels lower than the mean; and orange indicates expression level over the mean. (E) Biological canonical pathways that are potentially influenced by differentially expressed miRNAs. CT, control; OR, orange; PBMC, peripheral blood mononuclear cells.

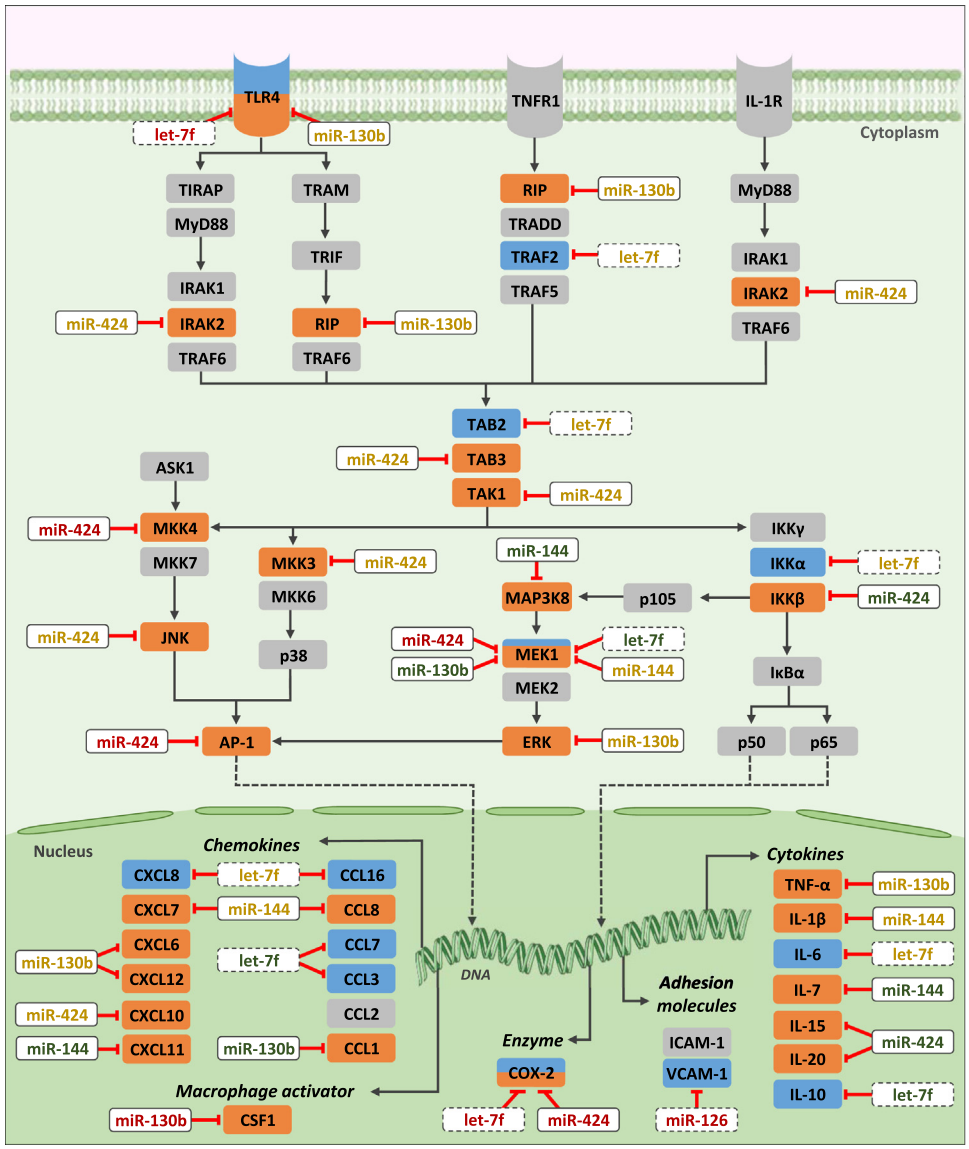

Fig. 4. Targets of differentially expressed miRNAs in the MAPK and NFκB signaling pathways in PBMC ($P<.05$), after daily intake of 500 mL of Moro orange juice for 4 weeks. Legend: orange box, protein with possible greater post-transcriptional silencing; blue box, protein with possible minor post-transcriptional silencing; orange and blue box, protein with possible highest (orange) and lowest (blue) post-transcriptional silencing according to the color gradient; gray box, possibly unmodulated protein; solid outline box, miRNA with increased expression; dashed outline box, miRNA with decreased expression; miRNA in red, experimentally validated target; miRNA in green, highly predicted target; miRNA in yellow, moderately predicted target. Targets obtained in silico in the IPA software. AP-1, activator protein 1; ASK1, apoptosis signal regulating kinase 1; CCL, C-C motif chemokine ligand; CSF1, colony stimulating factor 1; COX-2, Cyclooxygenase-2; CXCL, C-X-C motif chemokine ligand; ERK, extracellular signal-regulated kinase; IL, interleukin; IL-1R, interleukin-1 receptor; IKK, IκB kinase complex; ICAM-1, intercellular adhesion molecule 1; IκBα, nuclear factor kappa B inhibitor alpha; IRAK, interleukin-1 receptor-associated kinase; JNK, c-Jun N-terminal Kinase; p65, p50, and p105, nuclear factor kappa B subunits; MAP3K8, mitogen-activated protein kinase kinase kinase 8; MEK, ERK activator kinase; MKK, mitogen-activated protein kinase kinase; MyD88, myeloid differentiation primary response 88 protein; RIP, receptor-interacting protein; TLR4, toll like receptor 4; TNFR1, tumor necrosis factor receptor 1; TIRAP, toll/interleukin-1 receptor domain-containing adapter protein; TRAM, TRIF-related adaptor molecule; TRIF, toll-like receptor adapter molecule 1; TRADD, tumor necrosis factor receptor type 1-associated DEATH domain protein; TRAF, TNF receptor-associated factor; TAB, TAK1-binding protein; TAK1, transforming growth factor-beta-activated kinase 1; VCAM-1, vascular cell adhesion molecule 1; TNF-α, tumor necrosis factor-alpha.

pJNK/JNK ratio (P <.05) in PBMC samples (Fig. 5), corroborating the pathway analysis predictions. We did not find modulation of NFκB and STAT-3 in PMN (Supplementary Figure S7) or the inflammatory biomarkers analyzed (Table 5).

4. Discussion

Our findings show that regular BOJ intake modulated the expression of plasma and PBMC miRNAs related to the control of proteins expression of the MAPK and NFκB signaling pathways in overweight and insulin-resistant women following a Western dietary pattern. The intervention also reduced the expression of *IL6* mRNA and NFκB p65 subunit protein and increased the pJNK/JNK ratio in PBMC, as well as promoting the intake of vitamin C, flavonoids, and carotenoids. Conversely, there were no differences in the NFκB and STAT3-protein expression in PMN. Additionally, this supplementation did not result in significant or unhealthy changes in caloric intake, anthropometric analysis, or biochemical, hemodynamic, or hematological parameters assessed at the end of the experimental protocol.

Although the biochemical parameters remained within healthy levels ranges, the increase in LDL-cholesterol after the beverage

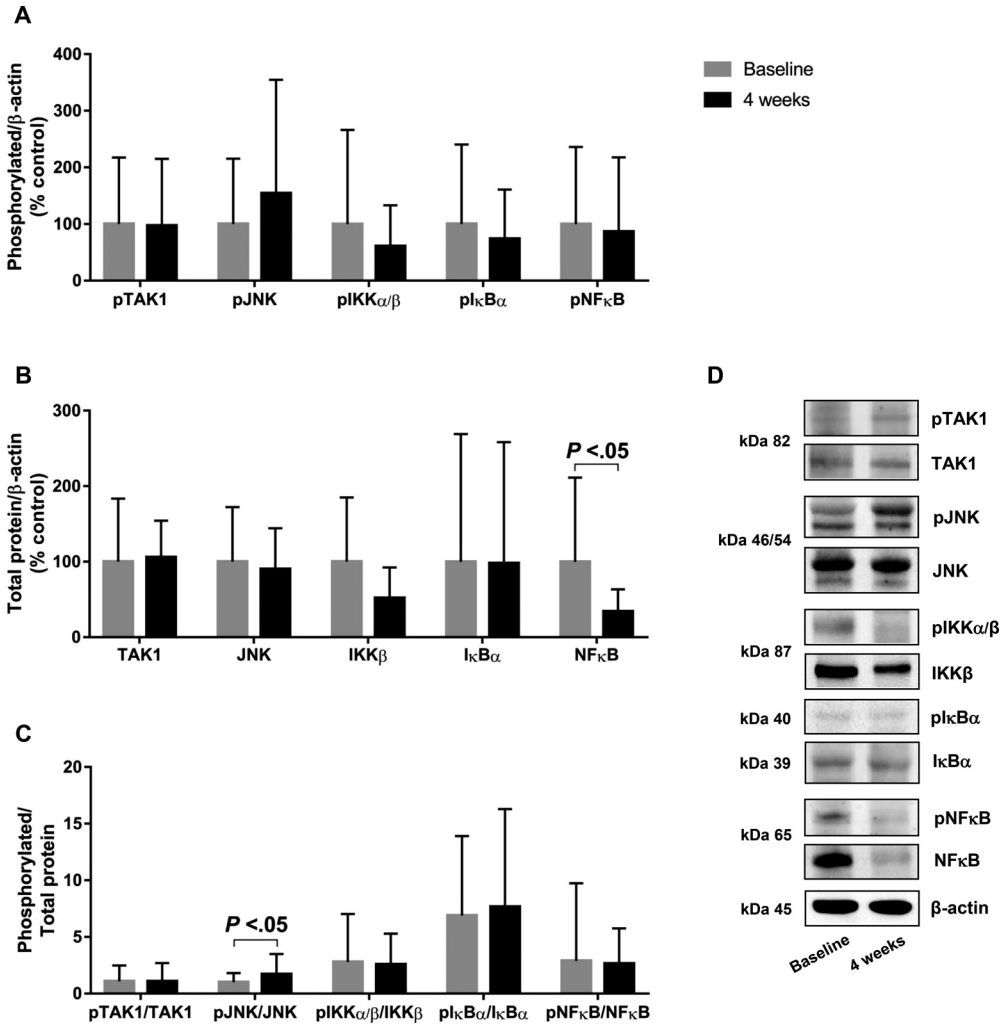

Fig. 5. Effect of Moro blood orange juice intake on the phosphorylation and expression of the proteins of the MAPK and NFκB signaling pathways in PBMC. (A) Phosphorylated and (B) total proteins (TAK1, JNK, IKKβ, IκBα, and NFκB) and (C) phosphorylated/total protein ratio were assessed through (D) protein expression images obtained by Western blotting. Values are mean±standard deviation (SD), n=12. Analyzed by paired t-test or Wilcoxon matched-pairs test. IKKβ, IκB kinase beta; IκBα, nuclear factor-kappa B inhibitor alpha; JNK, c-Jun N-terminal Kinase; and NFκB, nuclear factor kappa B p65 subunit; TAK1, transforming growth factor-beta-activated kinase 1.

intervention was intriguing. On the other hand, Hollands et al. [85] showed that ingestion of 500 mL/d of BOJ for 28 d did not change LDL-cholesterol levels in predominantly overweight Caucasian adults. However, Azzini et al. [34] showed a decrease in cholesterol and LDL-cholesterol levels after 12 weeks of supplementation with 500 mL/d of BOJ in obese women. This suggests that for a longer period of intake, BOJ can decrease and maintain healthy levels of LDL-c and, consequently, non-HDL cholesterol. Regarding the transaminase levels, although no studies were found that evaluated these enzymes after the intervention with BOJ, Gonçalves et al. [86] showed that in subjects with hepatitis C, supplementation with 500 mL/d of Pera orange juice for 8 weeks reduced AST levels. Thus, a longer period of intervention is suggested to assess the effect of BOJ on AST levels and the ALT/AST ratio in overweight individuals, especially when associated with liver diseases or the use of drugs and alcohol.

BOJ may have presented an important antioxidant contribution. The ORAC and DPPH assays showed that the beverage provided greater antioxidant capacity when compared to other juices, such as Cara Cara and Bahia orange juices, analyzed before and after pasteurization in a previous study [87]. In healthy smokers, acute BOJ intake increased the serum activity of glutathione peroxidase (GPx) [35]. Ribeiro et al. [88] showed that BOJ intake for 4 weeks at *ad libitum* attenuated doxorubicin-induced myocardial oxidative damage and improved glutathione peroxidase and catalase activity in rats. This antioxidant capacity of the BOJ is associated with the concentration of total phenolics, flavonoids, and vitamin C [32,89,90]. Particularly, citrus flavonoids are widely associated with antioxidant activity [24], such as demonstrated in PBMC, in which hesperidin and naringenin suppressed ROS generation by more than 50% and 70%, respectively [90].

Previous studies have shown that some BOJ compounds, such as vitamin C, hesperidin, didymin, lutein, and zeaxanthin, are also associated with the control of miRNAs expression [38–41]. Our data showed that BOJ intake upregulated the miR-144-3p expression in plasma, a miRNA widely expressed in human tissues and body fluids [91]. Alterations in plasma miR-144 levels were observed in NCD, and its plasma level was suggested as a biomarker for T2D and insulin resistance [92,93]. However, there are conflicting results regarding plasma miR-144 expression in T2D. For example, in a study with diabetic subjects, increased plasma miR-144 was associated with T2D in Swedes but not in Iraqis [94]. In addition, upregulation of plasma miR-144 levels may be appropriate in CVD. In diabetic patients with cardiac dysfunction, plasma miR-

Table 5
Plasma and serum metabolic profile analyzed at baseline and 4 weeks after daily ingestion of 500 mL of Moro blood orange juice

	Baseline	4 wk	*P*-value
Glucose (mg/dL)	80.0±12.4	75.8±11.4	.32
Insulinemia (μUI/mL)	15.2±5.8	14.5±4.5	.60
HOMA-IR	3.05±1.5	2.69±0.86	.23
Adiponectin (pg/mL)	5.29±2.52	5.08±2.30	.15
Leptin (pg/mL)	4.27±0.16	4.28±0.15	.90
Total cholesterol (mg/dL)	138±40	153±31	.06
HDL-cholesterol (mg/dL)	48.4±14.8	50.9±13.7	.42
LDL-cholesterol (mg/dL)	72.8±27.3	81.7±22.3	.04
Triacylglycerol (mg/dL)	86.5±41.4	95.8±46.7	.38
Non-HDL cholesterol (mg/dL)	90.0±33.4	101.6±28.7	.03
ALT (U/L)	12.8±6.1	12.7±4.2	.89
AST (U/L)	15.1±4.8	21.3±9.7	.01
AST/ALT ratio	1.28±0.38	1.73±0.70	<.01
GGT (U/L)	13.8±6.1	15.1±5.2	.14
White Blood Cells ($x10^3/mm^3$)	7.16±1.66	7.88±1.68	.16
LPS (EU/mL)	0.08±0.04	0.08±0.04	>.99
sCD14 (μg/mL)	2.06±0.32	2.02±0.34	.52
LBP (μg/mL)	13.4±4.1	13.1±4.6	.48
CRP (mg/L)	3.65±5.37	3.03±3.53	.94
Fibrinogen (mg/dL)	287±73	282±79	.21
D-dimer (ng/mL)	484±282	442±200	.37
IL-6 (pg/mL)	27.1±27.0	29.5±33.9	.43
IL-10 (pg/mL)	32.6±20.0	35.8±20.0	.90
TNF-α (pg/mL)	3.76±1.60	3.59±0.91	.56
sICAM (ng/mL)	341±89	320±80	.20
sVCAM (ng/mL)	395±123	374±110	.20
MCP-1 (pg/mL)	17.2±5.6	16.9±5.3	.78

All values are mean±standard deviation (SD), n=20.
Analyzed by paired t-test or Wilcoxon matched-pairs test.
Abbreviations: ALT, aspartate transaminase; AST, alanine transaminase; CRP, C-reactive protein; GGT, gamma-glutamyltransferase; HDL, high-density lipoprotein; HOMA-IR, Homeostasis model assessment of insulin resistance; IL, interleukin; LDL, low-density lipoprotein; MCP-1, monocyte chemoattractant protein-1; sCD14, Soluble cluster of differentiation 14; LPS, Lipopolysaccharide; LBP, Lipopolysaccharide binding protein; TNF-α, tumor necrosis factor-alpha; sICAM, soluble intercellular adhesion molecule; sVCAM, soluble vascular cell adhesion molecule.

144 levels were found to be markedly decreased, and plasma miR-144 overexpression in diabetes mice by agomiR protected the heart from hyperglycemia-induced lesions and promoted cardiac mitochondrial biogenesis [95].

MiR-144-3p was also upregulated in PBMC due to BOJ intake. Computational analysis revealed no experimentally validated targets for miR-144 in the MAPK and NFκB pathways. We identified as predicted targets of miR-144 the mRNAs of MAP3K8, IL-7, CXCL11, and TNF superfamily member (TNFSF) 11. Previously it was shown that the reduction of TNFSF11 by miR-144 results in decreased expression of TNF-α, IL-1β, IL-6, and IL-23 in dendritic cells and IL-17 in Th17 cells [96]. Taken together, these effects demonstrate that mir-144 may play an important role in attenuating the inflammatory response.

BOJ intake also upregulated miR-424-5p expression in PBMC. This miRNA has as experimentally validated targets MEK1, MKK4, AP-1, COX-2, and TNFSF9, and as highly predicted targets IKKβ, IL-20, and IL-15, and other genes of the MAPK and NFκB pathways. Among these targets, our results showed a slight decrease in IKKβ protein expression, but this was not statistically significant (P =.07). Moreover, miR-424 overexpression was associated with protection against LPS-induced inflammation [97,98]. Lee et al. [97] demonstrated that mice with endothelial-specific deletion of miR-322 (miR-424 ortholog) had increased angiogenic signaling in response to LPS via inflammatory processes.

MiR-424 may also be indirectly related to the control of intracellular protein phosphorylation in inflammatory pathways. Our in silico analysis showed that protein phosphatase 2A (PP2A) is an experimentally validated target of miR-424. PP2A is an enzyme responsible for controlling the phosphorylation of several intracellular proteins, including MAPK and NFκB pathway components, among which PP2A can dephosphorylate JNK [99]. Thus, the increased expression of miR-424 can potentially reduce the level of PP2A and, consequently, influence signaling pathways in which PP2A plays through a protein dephosphorylation mechanism.

BOJ intake did not increase JNK phosphorylation compared to the control. However, when we evaluated the phospho-JNK/JNK ratio, we found an increase in the proportion of phospho-JNK compared to the level of intracellular JNK. Although JNK phosphorylation is related to increased expression of inflammatory genes, cell death, and insulin resistance, JNK phosphorylation is also responsible for activation of the nuclear factor erythroid 2-related factor 2 (NRF2), which modulates the expression of antioxidant enzymes [100,101]. *In vitro*, the treatment of hepatocytes and neurons with the citrus flavanones neohesperidin (10–30 μM) and hesperetin (50 μM), respectively, increased JNK phosphorylation without decreasing cell viability [100,102]. Furthermore, pre-treatment of macrophages with lutein (10 μM) did not reduce LPS-induced JNK phosphorylation, although it resulted in decreased inflammatory stimulus by blocking LPS-induced phosphorylation of ERK and p38 kinases and TNF-α release [103]. Therefore, it is suggested that the increased proportion of phosphorylated JNK in PBMC due to BOJ intake is not associated with increased inflammatory activity or the development of insulin resistance but rather indicates one of the mechanisms by which BOJ plays an antioxidant protection role.

MiR-130b-3p was also upregulated in PBMC due to BOJ intake. In silico analysis indicated colony-stimulating factor 1 (CSF1) as an experimentally validated target and MEK1, CCL1, and IL10 receptor (IL10RB) as highly predicted targets of miR-130b, in addition to other targets in the inflammatory pathway with which this miRNA can bind moderately. Wang et al. [104] showed that upregulation of miR-130b attenuated LPS-induced inflammation in the lung of mice by binding to MAP3K8 mRNA; consequently, it decreased the expression of TNF-α, IL-6, and E-selectin, which resulted in the protection of the pulmonary vascular endothelium. Guo et al. [105] showed that miR-130b-3p also inhibited the polarization of macrophages M1 through the inhibition of the interferon regulatory factor 1 (IRF1), with a consequent reduction in the expression of the genes CCL5, CXCL10, enzyme inducible nitric oxide synthase (INOS), and TNF-α.

At the end of the experimental protocol, we observed a downregulation of let-7f-5p expression in PBMC. This miRNA has as experimentally validated targets the TLR4 and COX-2 mRNAs and as highly predicted targets the MEK1, IL-10, CCL3, -7, TNFSF9, and TNFSF10 mRNAs. However, our data show that the downregulation of let-7f-5p expression did not significantly increase plasma levels of IL-10. On the other hand, let-7f-5p downregulation may be useful to improve the insulin intracellular signaling, since let-7f targets the insulin receptor (INSR), insulin-like growth factor receptor 1 (IGF1R), insulin receptor substrate 2 (IRS-2), phosphatidylinositol 3 kinase interaction protein 1 (PIK3IP1), and protein kinase B/Akt 2 (Akt2) [106].

MiRNA let-7 clusters were identified as a factor important in controlling IL-6 expression. Mechanistically, let-7adf promotes IL-6 secretion by directly repressing tet methylcytosine dioxygenase 2 (Tet2) levels, an epigenetic regulator that removes methyl groups

from DNA, and indirectly by enhancing a Tet2 suppressor, succinate. Conversely, inhibition of let-7 expression increased Tet2 expression and decreased IL6 expression in macrophages. However, it is unclear how this modulating DNA demethylation can control IL-6 expression [107]. Interestingly, vitamin C was associated with the induction of Tet2 activity [108]. Consequently, it is speculated that vitamin C and the downregulation of let-7f-5p might lead to an anti-inflammatory effect. Therefore, this suggests that the decrease in IL6 mRNA levels after BOJ intake may be due to let-7f-5p downregulation and vitamin C intake. However, no change in IL-6 plasma levels was observed, which throughout our experimental protocol remained below the values found in overweight individuals, in whom the plasma level of IL-6 was on average 80 pg/mL [109].

The let-7 family is also related to the control of the NFκB pathway [46,47]. In silico analysis indicated that let-7f-5p and 130b-3p are highly predicted to target the homeobox protein Hox-B1 (HOXB1), a transcriptional regulator involved in the attenuation of p50 and p65 expression [110]. In our study, BOJ intake reduced the level of the NFκB p65 subunit. These results show that BOJ ingestion modulated the expression of miRNAs, which are indirectly involved in controlling p50 and p65 expression. On the other hand, there was no reduction in p65 mRNA levels, indicating only a post-transcriptional control at the protein level. Sirotkin et al. [45] showed that the main post-transcriptional inhibitors of p65 expression are miR-1, miR-27a, and miR-150. In our study, only miR-27a expression was assessed in all PBMC samples, but it did not show a significant upregulation (fold-change 1.22 and P=.09) at the end of the experimental protocol. Thus, the mechanism by which BOJ intake reduced the intracellular level of p65 in PBMC is unclear.

MiR-126-3p expression was also downregulated in PBMC at the end of the experimental protocol. In silico analysis indicated that miR-126 targets only VCAM-1 as an experimentally validated target and TNF receptor superfamily member 10b (TNFRSF10B) as a highly predicted target. In our analysis, the plasma VCAM-1 level did not change after BOJ intake, suggesting that the miR-126-3p downregulation may not have affected the expression of VCAM-1. Conversely, Yu et al. [111] showed that inhibition of miR-126 in chondrocytes reduced IL-1β-induced inflammation and increased the protein expression of the apoptosis regulator Bcl-2 (Bcl-2) through the inactivation of JNK and p38 pathways, with a consequent decrease in the content of IL-6, IL-8, and TNF-α. Furthermore, miR-126 downregulation in insulin-dependent cells may be helpful in T2D as it favors intracellular insulin signaling once that miR-126 targets IRS-1 [112] and IRS-2 [113].

Overall, the miRNA modulation previously mentioned may lead to a decrease in the inflammatory response by direct post-transcriptional control of proteins of the MAPK and NFκB signaling pathways and, indirectly, by control of transcription factors and enzymes that can regulate the expression and activity of specific pathway components. Although no change was observed in the inflammatory biomarkers, our results suggest that the changes observed at the molecular level may be part of the early control mechanisms at the inflammatory signaling pathway, promoted by the regular BOJ intake. Further studies are needed to elucidate the mechanism responsible for the decrease of p65 level by the beverage intake. Certainly, this will support the use of Moro blood orange in nutritional therapies, which can be useful in the risk reduction and management of NCD.

Author contributions

Conceptualization and methodology, V.C.C., B.J.Q., and M.M.R.; Investigation, V.C.C.; B.J.Q., D.C.O., A.H.N., L.A.M., and G.R.S.; Formal analysis and data curation, V.C.C., F.M.F., R.A.F., A.H.N., and L.R.P.F.; Supervision, M.M.R.; Writing - Original draft, V.C.C.; Writing - Review and editing, V.C.C., M.M.R., R.A.F., L.R.P.F., N.M.A.H. and F.M.L.; and Final approval, all authors.

Funding

This work was supported by FAPESP (grant 2013/07914-8 and 2018/25046-7) and FAPEMIG (grant APQ-03608-17).

Declaration of Competing Interest

The authors declare that there are no conflicts of interest.

Acknowledgment

We are indebted to all volunteers from the study, the staff at Health Center Geraldo Horacio de Paula Souza for their invaluable contribution, Fundecitrus for the donation of blood orange juice (BOJ), and São Paulo Research Foundation (FAPESP) and Minas Gerais Research Foundation (FAPEMIG) for their financial support.

This work was supported by FAPESP (grant 2013/07914-8 and 2018/25046-7) and FAPEMIG (grant APQ-03608-17).

Supplementary materials

Supplementary material associated with this article can be found, in the online version, at doi:10.1016/j.jnutbio.2022.109240.

References

[1] WHO. Obesity and overweight 2021.
[2] Senthilingam M. Covid-19 has made the obesity epidemic worse, but failed to ignite enough action. BMJ 2021;372:n411. doi:10.1136/bmj.n411.
[3] Monteiro CA, Cannon G, Levy RB, Moubarac J-C, Louzada ML, Rauber F, et al. Ultra-processed foods: what they are and how to identify them. Public Health Nutr 2019;22:936–41. doi:10.1017/S1368980018003762.
[4] Christ A, Lauterbach M, Latz E. Western diet and the immune system: an inflammatory connection. Immunity 2019;51:794–811. doi:10.1016/j.immuni.2019.09.020.
[5] Cooper-Capetini V, de Vasconcelos DAA, Martins AR, Hirabara SM, Donato J, Carpinelli AR, et al. Zinc supplementation improves glucose homeostasis in high fat-fed mice by enhancing pancreatic β-cell function. Nutrients 2017;9:E1150. doi:10.3390/nu9101150.
[6] Quintanilha BJ, Pinto Ferreira LR, Ferreira FM, Neto EC, Sampaio GR, Rogero MM. Circulating plasma microRNAs dysregulation and metabolic endotoxemia induced by a high-fat high-saturated diet. Clin Nutr 2020;39:554–62. doi:10.1016/j.clnu.2019.02.042.
[7] González F, Considine RV, Abdelhadi OA, Acton AJ. Saturated fat ingestion promotes lipopolysaccharide-mediated inflammation and insulin resistance in polycystic ovary syndrome. J Clin Endocrinol Metab 2019;104:934–46. doi:10.1210/jc.2018-01143.
[8] Kochumon S, Wilson A, Chandy B, Shenouda S, Tuomilehto J, Sindhu S, et al. Palmitate Activates CCL4 expression in human monocytic cells via TLR4/MyD88 dependent activation of NF-κB/MAPK/PI3K signaling systems. Cell Physiol Biochem 2018;46:953–64. doi:10.1159/000488824.
[9] Hussey SE, Liang H, Costford SR, Klip A, DeFronzo RA, Sanchez-Avila A, et al. TAK-242, a small-molecule inhibitor of Toll-like receptor 4 signalling, unveils similarities and differences in lipopolysaccharide- and lipid-induced inflammation and insulin resistance in muscle cells. Biosci Rep 2012;33:37–47. doi:10.1042/BSR20120098.
[10] Rogero MM, Calder PC. Obesity, inflammation, toll-like receptor 4 and fatty acids. Nutrients 2018;10:E432. doi:10.3390/nu10040432.
[11] Lancaster GI, Langley KG, Berglund NA, Kammoun HL, Reibe S, Estevez E, et al. Evidence that TLR4 is not a receptor for saturated fatty acids but mediates lipid-induced inflammation by reprogramming macrophage metabolism. Cell Metab 2018;27:1096–110 e5.. doi:10.1016/j.cmet.2018.03.014.
[12] Robblee MM, Kim CC, Porter Abate J, Valdearcos M, Sandlund KLM, Shenoy MK, et al. Saturated fatty acids engage an IRE1α-dependent pathway to activate the NLRP3 inflammasome in myeloid cells. Cell Rep 2016;14:2611–23. doi:10.1016/j.celrep.2016.02.053.
[13] Roma LP, Jonas J-C. Nutrient metabolism, subcellular redox state, and oxidative stress in pancreatic islets and β-cells. J Mol Biol 2020;432:1461–93. doi:10.1016/j.jmb.2019.10.012.

[14] Thomas D, Apovian C. Macrophage functions in lean and obese adipose tissue. Metabolism 2017;72:120–43. doi:10.1016/j.metabol.2017.04.005.
[15] Talukdar S, Oh DY, Bandyopadhyay G, Li D, Xu J, McNelis J, et al. Neutrophils mediate insulin resistance in mice fed a high-fat diet through secreted elastase. Nat Med 2012;18:1407–12. doi:10.1038/nm.2885.
[16] Hadad N, Burgazliev O, Elgazar-Carmon V, Solomonov Y, Wueest S, Item F, et al. Induction of cytosolic phospholipase a2α is required for adipose neutrophil infiltration and hepatic insulin resistance early in the course of high-fat feeding. Diabetes 2013;62:3053–63. doi:10.2337/db12-1300.
[17] Hotamisligil GS. Inflammation and metabolic disorders. Nature 2006;444:860–7. doi:10.1038/nature05485.
[18] van Meijl LEC, Mensink RP. Effects of low-fat dairy consumption on markers of low-grade systemic inflammation and endothelial function in overweight and obese subjects: an intervention study. Br J Nutr 2010;104:1523–7. doi:10.1017/S0007114510002515.
[19] Halle M, Korsten-Reck U, Wolfarth B, Berg A. Low-grade systemic inflammation in overweight children: impact of physical fitness. Exerc Immunol Rev 2004;10:66–74.
[20] Visser M, Bouter LM, McQuillan GM, Wener MH, Harris TB. Elevated C-reactive protein levels in overweight and obese adults. JAMA 1999;282:2131–5. doi:10.1001/jama.282.22.2131.
[21] Trautwein EA, McKay S. The role of specific components of a plant-based diet in management of dyslipidemia and the impact on cardiovascular risk. Nutrients 2020;12:E2671. doi:10.3390/nu12092671.
[22] Kim H, Lee K, Rebholz CM, Kim J. Plant-based diets and incident metabolic syndrome: results from a South Korean prospective cohort study. PLoS Med 2020;17:e1003371. doi:10.1371/journal.pmed.1003371.
[23] Ghanim H, Sia CL, Upadhyay M, Upadhyay M, Korzeniewski K, Viswanathan P, et al. Orange juice neutralizes the proinflammatory effect of a high-fat, high-carbohydrate meal and prevents endotoxin increase and Toll-like receptor expression. Am J Clin Nutr 2010;91:940–9. doi:10.3945/ajcn.2009.28584.
[24] Gattuso G, Barreca D, Gargiulli C, Leuzzi U, Caristi C. Flavonoid composition of Citrus juices. Molecules 2007;12:1641–73. doi:10.3390/12081641.
[25] Brett GM, Hollands W, Needs PW, Teucher B, Dainty JR, Davis BD, et al. Absorption, metabolism and excretion of flavanones from single portions of orange fruit and juice and effects of anthropometric variables and contraceptive pill use on flavanone excretion. Br J Nutr 2009;101:664–75. doi:10.1017/S000711450803081X.
[26] Cebadera-Miranda L, Domínguez L, Dias MI, Barros L, Ferreira ICFR, Igual M, et al. Sanguinello and Tarocco (Citrus sinensis [L.] Osbeck): bioactive compounds and colour appearance of blood oranges. Food Chem 2019;270:395–402. doi:10.1016/j.foodchem.2018.07.094.
[27] Grosso G, Galvano F, Mistretta A, Marventano S, Nolfo F, Calabrese G, et al. Red orange: experimental models and epidemiological evidence of its benefits on human health. Oxid Med Cell Longev 2013;2013:157240. doi:10.1155/2013/157240.
[28] Parhiz H, Roohbakhsh A, Soltani F, Rezaee R, Iranshahi M. Antioxidant and anti-inflammatory properties of the citrus flavonoids hesperidin and hesperetin: an updated review of their molecular mechanisms and experimental models. Phytother Res 2015;29:323–31. doi:10.1002/ptr.5256.
[29] Sun Y, Li L. Cyanidin-3-glucoside inhibits inflammatory activities in human fibroblast-like synoviocytes and in mice with collagen-induced arthritis. Clin Exp Pharmacol Physiol 2018;45:1038–45. doi:10.1111/1440-1681.12970.
[30] Bian Q, Gao S, Zhou J, Qin J, Taylor A, Johnson EJ, et al. Lutein and zeaxanthin supplementation reduces photooxidative damage and modulates the expression of inflammation-related genes in retinal pigment epithelial cells. Free Radic Biol Med 2012;53:1298–307. doi:10.1016/j.freeradbiomed.2012.06.024.
[31] Ellulu MS, Rahmat A, Patimah I, Khaza'ai H, Abed Y. Effect of vitamin C on inflammation and metabolic markers in hypertensive and/or diabetic obese adults: a randomized controlled trial. Drug Des Devel Ther 2015;9:3405–12. doi:10.2147/DDDT.S83144.
[32] Arena E, Fallico B, Maccarone E. Evaluation of antioxidant capacity of blood orange juices as influenced by constituents, concentration process and storage. Food Chemistry 2001;74:423–7. doi:10.1016/S0308-8146(01)00125-X.
[33] Li L, Lyall GK, Martinez-Blazquez JA, Vallejo F, A Tomas-Barberan F, Birch KM, et al. Blood orange juice consumption increases flow-mediated dilation in adults with overweight and obesity: a randomized controlled trial. J Nutr 2020;150:2287–94. doi:10.1093/jn/nxaa158.
[34] Azzini E, Venneria E, Ciarapica D, Foddai MS, Intorre F, Zaccaria M, et al. Effect of red orange juice consumption on body composition and nutritional status in overweight/obese female: a pilot study. Oxid Med Cell Longev 2017;2017:1672567. doi:10.1155/2017/1672567.
[35] Dorna MS, Barbosa EMS, Callegari MA, Tanni SE, Chiuso-Minicucci F, Felix TF, et al. Orange juice attenuates circulating miR-150-5p, miR-25-3p, and miR-451a in healthy smokers: a randomized crossover study. Front Nutr 2021;8:1210. doi:10.3389/fnut.2021.775515.
[36] Cardile V, Graziano ACE, Venditti A. Clinical evaluation of Moro (Citrus sinensis (L.) Osbeck) orange juice supplementation for the weight management. Nat Prod Res 2015;29:2256–60. doi:10.1080/14786419.2014.1000897.
[37] Milenkovic D, Jude B, Morand C. miRNA as molecular target of polyphenols underlying their biological effects. Free Radic Biol Med 2013;64:40–51. doi:10.1016/j.freeradbiomed.2013.05.046.
[38] Singhal SS, Singhal S, Singhal P, Singhal J, Horne D, Awasthi S. Didymin: an orally active citrus flavonoid for targeting neuroblastoma. Oncotarget 2017;8:29428–41. doi:10.18632/oncotarget.15204.
[39] Shojania HR, Momeni-Moghaddam M, Hossini S-E, Armin M, Omrani Bidi J. MicroRNA 155 downregulation by vitamin C-loaded human serum albumin nanoparticles during cutaneous wound healing in mice. Int J Low Extrem Wounds 2019;18:143–52. doi:10.1177/1534734619842975.
[40] Li X, Sun M, Long Y. Cyanidin-3-O-glucoside attenuates lipopolysaccharide-induced inflammation in human corneal epithelial cells by inducing Let-7b-5p-Mediated HMGA2/PI3K/Akt pathway. Inflammation 2020;43:1088–96. doi:10.1007/s10753-020-01194-0.
[41] Kim J, Lee J, Oh JH, Chang HJ, Sohn DK, Kwon O, et al. Dietary lutein plus zeaxanthin intake and DICER1 rs3742330 A>G polymorphism relative to colorectal cancer risk. Sci Rep 2019;9:3406. doi:10.1038/s41598-019-39747-5.
[42] Capetini VC, Quintanilha BJ, Sampaio GR, Ferreira FM, Rogero M. Blood orange juice intake modulates the expression of miR-126–3p and let-7f-5p in PBMC of overweight and insulin resistance women. Curr Dev Nutr 2021;5:936. doi:10.1093/cdn/nzab050_003.
[43] Friedman RC, Farh KK-H, Burge CB, Bartel DP. Most mammalian mRNAs are conserved targets of microRNAs. Genome Res 2009;19:92–105. doi:10.1101/gr.082701.108.
[44] Zhong L, Simard MJ, Huot J. Endothelial microRNAs regulating the NF-κB pathway and cell adhesion molecules during inflammation. FASEB J 2018;32:4070–84. doi:10.1096/fj.201701536R.
[45] Sirotkin AV, Alexa R, Kišová G, Harrath AH, Alwasel S, Ovcharenko D, et al. MicroRNAs control transcription factor NF-kB (p65) expression in human ovarian cells. Funct Integr Genomics 2015;15:271–5. doi:10.1007/s10142-014-0413-0.
[46] Kumar M, Sahu SK, Kumar R, Subuddhi A, Maji RK, Jana K, et al. MicroRNA let-7 modulates the immune response to mycobacterium tuberculosis infection via control of A20, an inhibitor of the NF-κB pathway. Cell Host Microbe 2015;17:345–56. doi:10.1016/j.chom.2015.01.007.
[47] Liu J, Zhu L, Xie G, Bao J, Yu Q. Let-7 miRNAs modulate the activation of NF-κB by Targeting TNFAIP3 and are involved in the pathogenesis of lupus nephritis. PLoS One 2015;10:e0121256. doi:10.1371/journal.pone.0121256.
[48] Mori MA, Ludwig RG, Garcia-Martin R, Brandão BB, Kahn CR. Extracellular miRNAs: from biomarkers to mediators of physiology and disease. Cell Metab 2019;30:656–73. doi:10.1016/j.cmet.2019.07.011.
[49] Zhang J, Li S, Li L, Li M, Guo C, Yao J, et al. Exosome and exosomal microRNA: trafficking, sorting, and function. Genom Proteomics Bioinform 2015;13:17–24. doi:10.1016/j.gpb.2015.02.001.
[50] Van Meter EN, Onyango JA, Teske KA. A review of currently identified small molecule modulators of microRNA function. Eur J Med Chem 2020;188:112008. doi:10.1016/j.ejmech.2019.112008.
[51] Donate PB, Lima KA de, Peres RS, Almeida F, Fukada SY, Silva TA, et al. Cigarette smoke induces miR-132 in Th17 cells that enhance osteoclastogenesis in inflammatory arthritis. PNAS 2021;118. doi:10.1073/pnas.2017120118.
[52] Quintanilha BJ, Reis BZ, Duarte GBS, Cozzolino SMF, Rogero MM. Nutrimiromics: role of microRNAs and nutrition in modulating inflammation and chronic diseases. Nutrients 2017;9:E1168. doi:10.3390/nu9111168.
[53] Quintanilha BJ, Chaves DFS, Brasili E, Corrêa TAF, Capetini VC, Ferreira FM, et al. Ingestion of orange juice prevents hyperglycemia and increases plasma miR-375 expression. Clinical Nutrition ESPEN 2021;0. doi:10.1016/j.clnesp.2021.12.003.
[54] Chaudhary R, Dubey A, Sonker A. Techniques used for the screening of hemoglobin levels in blood donors: current insights and future directions. J Blood Med 2017;8:75–88. doi:10.2147/JBM.S103788.
[55] NEPA/UNICAMP. Campinas: Núcleo de Estudos e Pesquisas em Alimentação - NEPA/UNICAMPTabela Brasileira de Composição de Alimentos – TACO. 4th ed; 2011.
[56] U.S. Department of Agriculture, Agricultural research service. FoodData Central 2019. fdc.nal.usda.gov (accessed 10 January, 2021).
[57] IOM. DRI Dietary reference intakes: applications in dietary assessment. Washington (DC): National Academies Press (US); 2002.
[58] Swain T, Hillis WE. The phenolic constituents of Prunus domestica. I.—The quantitative analysis of phenolic constituents. J Sci Food Agric 1959;10:63–8. doi:10.1002/jsfa.2740100110.
[59] Pasternak T, Potters G, Caubergs R, Jansen MAK. Complementary interactions between oxidative stress and auxins control plant growth responses at plant, organ, and cellular level. J Exp Bot 2005;56:1991–2001. doi:10.1093/jxb/eri196.
[60] Shiga TM, Soares CA, Nascimento JR, Purgatto E, Lajolo FM, Cordenunsi BR. Ripening-associated changes in the amounts of starch and non-starch polysaccharides and their contributions to fruit softening in three banana cultivars. J Sci Food Agric 2011;91:1511–16. doi:10.1002/jsfa.4342.
[61] AOAC Official methods of analysis of AOAC international. 16th ed. Arlington: VA: Association of Official Analytical Chemists (AOAC); 1995.
[62] Prior RL, Hoang H, Gu L, Wu X, Bacchiocca M, Howard L, et al. Assays for hydrophilic and lipophilic antioxidant capacity (oxygen radical absorbance capacity (ORAC(FL))) of plasma and other biological and food samples. J Agric Food Chem 2003;51:3273–9. doi:10.1021/jf0262256.

[63] Brand-Williams W, Cuvelier ME, Berset C. Use of a free radical method to evaluate antioxidant activity. LWT - Food Sci Technol 1995;28:25–30. doi:10.1016/S0023-6438(95)80008-5.

[64] Nishioka A, Tobaruela E de C, Fraga LN, Tomás-Barberán FA, Lajolo FM, Hassimotto NMA. Stratification of volunteers according to flavanone metabolite excretion and phase II metabolism profile after single doses of "pera" orange and "moro" blood orange juices. Nutrients 2021;13:473. doi:10.3390/nu13020473.

[65] Petry FC, Mercadante AZ. New method for carotenoid extraction and analysis by HPLC-DAD-MS/MS in freeze-dried citrus and mango pulps. J Braz Chem Soc 2018;29:205–15. doi:10.21577/0103-5053.20170127.

[66] Matthews DR, Hosker JP, Rudenski AS, Naylor BA, Treacher DF, Turner RC. Homeostasis model assessment: insulin resistance and beta-cell function from fasting plasma glucose and insulin concentrations in man. Diabetologia 1985;28:412–19. doi:10.1007/BF00280883.

[67] Verbeek R, Hovingh GK, Boekholdt SM. Non-high-density lipoprotein cholesterol: current status as cardiovascular marker. Curr Opin Lipidol 2015;26:502–10. doi:10.1097/MOL.0000000000000237.

[68] Hall P, Cash J. What is the real function of the liver "function" tests? Ulster Med J 2012;81:30–6.

[69] Eggleton P. Separation of cells using free flow electrophoresis. In: Cell separation a practical approach. Oxford: Oxford University Press; 1998. p. 213–52.

[70] Wilfinger WW, Mackey K, Chomczynski P. Effect of pH and ionic strength on the spectrophotometric assessment of nucleic acid purity. Biotechniques 1997;22:478–81 474–6. doi:10.2144/97223st01.

[71] Livak KJ, Schmittgen TD. Analysis of relative gene expression data using real-time quantitative PCR and the 2(-Delta Delta C(T)) Method. Methods 2001;25:402–8. doi:10.1006/meth.2001.1262.

[72] Blondal T, Jensby Nielsen S, Baker A, Andreasen D, Mouritzen P, Wrang Teilum M, et al. Assessing sample and miRNA profile quality in serum and plasma or other biofluids. Methods 2013;59:S1–6. doi:10.1016/j.ymeth.2012.09.015.

[73] Chen Y, Yin Y, Jiang H. miR-30e-5p Alleviates Inflammation and cardiac dysfunction after myocardial infarction through targeting PTEN. Inflammation 2021;44:769–79. doi:10.1007/s10753-020-01376-w.

[74] Ye E-A, Liu L, Steinle JJ. miR-15a/16 inhibits TGF-beta3/VEGF signaling and increases retinal endothelial cell barrier proteins. Vision Res 2017;139:23–9. doi:10.1016/j.visres.2017.07.007.

[75] Zhao X, Li S, Wang Z, Bai N, Feng Y. miR–101–3p negatively regulates inflammation in systemic lupus erythematosus via MAPK1 targeting and inhibition of the NF–κB pathway. Mol Med Rep 2021;23:359. doi:10.3892/mmr.2021.11998.

[76] Ma Y, Liu Y, Hou H, Yao Y, Meng H. MiR-150 predicts survival in patients with sepsis and inhibits LPS-induced inflammatory factors and apoptosis by targeting NF-κB1 in human umbilical vein endothelial cells. Biochem Biophys Res Commun 2018;500:828–37. doi:10.1016/j.bbrc.2018.04.168.

[77] Xu G, Zhang Z, Wei J, Zhang Y, Zhang Y, Guo L, et al. microR-142-3p down-regulates IRAK-1 in response to Mycobacterium bovis BCG infection in macrophages. Tuberculosis (Edinb) 2013;93:606–11. doi:10.1016/j.tube.2013.08.006.

[78] Zhu D, Pan C, Li L, Bian Z, Lv Z, Shi L, et al. MicroRNA-17/20a/106a modulate macrophage inflammatory responses through targeting signal-regulatory protein α. J Allergy Clin Immunol 2013;132:426–36 .e8. doi:10.1016/j.jaci.2013.02.005.

[79] Ritchie ME, Phipson B, Wu D, Hu Y, Law CW, Shi W, et al. limma powers differential expression analyses for RNA-sequencing and microarray studies. Nucleic Acids Res 2015;43:e47. doi:10.1093/nar/gkv007.

[80] Shin C, Nam J-W, Farh KK-H, Chiang HR, Shkumatava A, Bartel DP. Expanding the microRNA targeting code: functional sites with centered pairing. Mol Cell 2010;38:789–802. doi:10.1016/j.molcel.2010.06.005.

[81] WHO. Waist circumference and waist-hip ratio: report of a WHO expert consultation 8-11 December2008.

[82] Geloneze B, Vasques ACJ, Stabe CFC, Pareja JC, Rosado LEFP de L, Queiroz EC de, et al. HOMA1-IR and HOMA2-IR indexes in identifying insulin resistance and metabolic syndrome: Brazilian Metabolic Syndrome Study (BRAMS). Arq Bras Endocrinol Metabol 2009;53:281–7. doi:10.1590/s0004-27302009000200020.

[83] WHO. Diet, nutrition and the prevention of chronic diseases: report of a joint WHO/FAO expert consultation 2003.

[84] Brunzell JD, Davidson M, Furberg CD, Goldberg RB, Howard BV, Stein JH, et al. Lipoprotein management in patients with cardiometabolic risk: consensus statement from the American Diabetes Association and the American College of Cardiology Foundation. Diabetes Care 2008;31:811–22. doi:10.2337/dc08-9018.

[85] Hollands WJ, Armah CN, Doleman JF, Perez-Moral N, Winterbone MS, Kroon PA. 4-Week consumption of anthocyanin-rich blood orange juice does not affect LDL-cholesterol or other biomarkers of CVD risk and glycaemia compared with standard orange juice: a randomised controlled trial. Br J Nutr 2018;119:415–21. doi:10.1017/S0007114517003865.

[86] Gonçalves D, Lima C, Ferreira P, Costa P, Costa A, Figueiredo W, et al. Orange juice as dietary source of antioxidants for patients with hepatitis C under antiviral therapy. Food Nutr Res 2017;61:1296675. doi:10.1080/16546628.2017.1296675.

[87] Brasili E, Chaves DFS, Xavier AAO, Mercadante AZ, Hassimotto NMA, Lajolo FM. Effect of Pasteurization on Flavonoids and Carotenoids in Citrus sinensis (L.) Osbeck cv. "Cara Cara" and "Bahia" Juices. J Agric Food Chem 2017;65:1371–7. doi:10.1021/acs.jafc.6b05401.

[88] Ribeiro APD, Pereira AG, Todo MC, Fujimori ASS, Dos Santos PP, Dantas D, et al. Pera orange (Citrus sinensis) and Moro orange (Citrus sinensis (L.) Osbeck) juices attenuate left ventricular dysfunction and oxidative stress and improve myocardial energy metabolism in acute doxorubicin-induced cardiotoxicity in rats. Nutrition 2021;91:111350 –92. doi:10.1016/j.nut.2021.111350.

[89] Tounsi MS, Wannes WA, Ouerghemmi I, Jegham S, Ben Njima Y, Hamdaoui G, et al. Juice components and antioxidant capacity of four Tunisian Citrus varieties. J Sci Food Agric 2011;91:142–51. doi:10.1002/jsfa.4164.

[90] Ghanim H, Mohanty P, Pathak R, Chaudhuri A, Sia CL, Dandona P. Orange juice or fructose intake does not induce oxidative and inflammatory response. Diabetes Care 2007;30:1406–11. doi:10.2337/dc06-1458.

[91] Sun L, Yu Y, Niu B, Wang D. Red blood cells as potential repositories of MicroRNAs in the circulatory system. Front Genet 2020;11:442. doi:10.3389/fgene.2020.00442.

[92] Liang Y-Z, Dong J, Zhang J, Wang S, He Y, Yan Y-X. Identification of Neuroendocrine Stress Response-Related Circulating MicroRNAs as Biomarkers for Type 2 Diabetes Mellitus and Insulin Resistance. Front Endocrinol (Lausanne) 2018;9:132. doi:10.3389/fendo.2018.00132.

[93] Zhu H, Leung SW. Identification of microRNA biomarkers in type 2 diabetes: a meta-analysis of controlled profiling studies. Diabetologia 2015;58:900–11. doi:10.1007/s00125-015-3510-2.

[94] Wang X, Sundquist J, Zöller B, Memon AA, Palmér K, Sundquist K, et al. Determination of 14 circulating microRNAs in Swedes and Iraqis with and without diabetes mellitus type 2. PLoS One 2014;9:e86792. doi:10.1371/journal.pone.0086792.

[95] Tao L, Huang X, Xu M, Yang L, Hua F. MiR-144 protects the heart from hyperglycemia-induced injury by regulating mitochondrial biogenesis and cardiomyocyte apoptosis. FASEB J 2020;34:2173–97. doi:10.1096/fj.201901838R.

[96] Li R-D, Shen C-H, Tao Y-F, Zhang X-F, Zhang Q-B, Ma Z-Y, et al. MicroRNA-144 suppresses the expression of cytokines through targeting RANKL in the matured immune cells. Cytokine 2018;108:197–204. doi:10.1016/j.cyto.2018.03.043.

[97] Lee A, Papangeli I, Park Y, Jeong H-N, Choi J, Kang H, et al. A PPARγ-dependent miR-424/503-CD40 axis regulates inflammation mediated angiogenesis. Sci Rep 2017;7:2528. doi:10.1038/s41598-017-02852-4.

[98] Cheng D, Zhu C, Liang Y, Xing Y, Shi C. MiR-424 overexpression protects alveolar epithelial cells from LPS-induced apoptosis and inflammation by targeting FGF2 via the NF-κB pathway. Life Sci 2020;242:117213. doi:10.1016/j.lfs.2019.117213.

[99] Clark AR, Ohlmeyer M. Protein phosphatase 2A as a therapeutic target in inflammation and neurodegeneration. Pharmacol Ther 2019;201:181–201. doi:10.1016/j.pharmthera.2019.05.016.

[100] Su C, Xia X, Shi Q, Song X, Fu J, Xiao C, et al. Neohesperidin Dihydrochalcone versus CCl_4-Induced Hepatic Injury through Different Mechanisms: The Implication of Free Radical Scavenging and Nrf2 Activation. J Agric Food Chem 2015;63:5468–75. doi:10.1021/acs.jafc.5b01750.

[101] Hu Y-R, Ma H, Zou Z-Y, He K, Xiao Y-B, Wang Y, et al. Activation of Akt and JNK/Nrf2/NQO1 pathway contributes to the protective effect of coptisine against AAPH-induced oxidative stress. Biomed Pharmacother 2017;85:313–22. doi:10.1016/j.biopha.2016.11.031.

[102] Hwang S-L, Yen G-C. Modulation of Akt, JNK, and p38 activation is involved in citrus flavonoid-mediated cytoprotection of PC12 cells challenged by hydrogen peroxide. J Agric Food Chem 2009;57:2576–82. doi:10.1021/jf8033607.

[103] Xagorari A, Roussos C, Papapetropoulos A. Inhibition of LPS-stimulated pathways in macrophages by the flavonoid luteolin. Br J Pharmacol 2002;136:1058–64. doi:10.1038/sj.bjp.0704803.

[104] Wang P, Zhang X, Li F, Yuan K, Li M, Zhang J, et al. MiR-130b attenuates vascular inflammation via negatively regulating tumor progression locus 2 (Tpl2) expression. Int Immunopharmacol 2017;51:9–16. doi:10.1016/j.intimp.2017.07.020.

[105] Guo Q, Zhu X, Wei R, Zhao L, Zhang Z, Yin X, et al. miR-130b-3p regulates M1 macrophage polarization via targeting IRF1. J Cell Physiol 2021;236:2008–22. doi:10.1002/jcp.29987.

[106] Zhu H, Shyh-Chang N, Segrè AV, Shinoda G, Shah SP, Einhorn WS, et al. The Lin28/let-7 axis regulates glucose metabolism. Cell 2011;147:81–94. doi:10.1016/j.cell.2011.08.033.

[107] Jiang S, Yan W, Wang SE, Baltimore D. Dual mechanisms of posttranscriptional regulation of Tet2 by Let-7 microRNA in macrophages. Proc Natl Acad Sci U S A 2019;116:12416–21. doi:10.1073/pnas.1811040116.

[108] Lindsey RC, Cheng S, Mohan S. Vitamin C effects on 5-hydroxymethylcytosine and gene expression in osteoblasts and chondrocytes: Potential involvement of PHD2. PLoS One 2019;14:e0220653. doi:10.1371/journal.pone.0220653.

[109] El-Mikkawy DME, EL-Sadek MA, EL-Badawy MA, Samaha D. Circulating level of interleukin-6 in relation to body mass indices and lipid profile in Egyptian adults with overweight and obesity. Egypt Rheumatol Rehabil 2020;47:7. doi:10.1186/s43166-020-00003-8.

[110] Zhou J-L, Deng S, Fang H-S, Yu G, Peng H. Hsa-let-7g promotes osteosarcoma by reducing HOXB1 to activate NF-kB pathway. Biomed Pharmacother 2019;109:2335–41. doi:10.1016/j.biopha.2018.11.026.
[111] Yu CD, Miao WH, Zhang YY, Zou MJ, Yan XF. Inhibition of miR-126 protects chondrocytes from IL-1β induced inflammation via upregulation of Bcl-2. Bone Joint Res 2018;7:414–21. doi:10.1302/2046-3758.76.BJR-2017-0138.R1.
[112] Fang S, Ma X, Guo S, Lu J. MicroRNA-126 inhibits cell viability and invasion in a diabetic retinopathy model via targeting IRS-1. Oncol Lett 2017;14:4311–18. doi:10.3892/ol.2017.6695.
[113] Tao H, Wang M, Zhang M, Zhang S, Wang C, Yuan W, et al. MiR-126 Suppresses the Glucose-Stimulated Proliferation via IRS-2 in INS-1 β Cells. PLoS One 2016;11:e0149954. doi:10.1371/journal.pone.0149954.